https://doi.org/10.5194/amt-2020-403
Preprint. Discussion started: 10 November 2020

Atmospheric Measurement Techniques Discussions

The Adaptable 4A Inversion (5AI): Description and first XCO_2 retrievals from OCO-2 observations

Matthieu Dogniaux[1], Cyril Crevoisier[1], Raymond Armante[1], Virginie Capelle[1], Thibault Delahaye[1], Vincent Cassé[1], Martine De Mazière[2], Nicholas M. Deutscher[3,4], Dietrich G. Feist[5,6,7], Omaira E. Garcia[8], David W. T. Griffith[3], Frank Hase[9], Laura T. Iraci[10], Rigel Kivi[11], Isamu Morino[12], Justus Notholt[4], David F. Pollard[13], Coleen M. Roehl[14], Kei Shiomi[15], Kimberly Strong[16], Yao Té[17], Voltaire A. Velazco[3], Thorsten Warneke[4]

[1]Laboratoire de Météorologie Dynamique/IPSL, CNRS, École polytechnique, Institut Polytechnique de Paris, Sorbonne Université, École Normale Supérieure, PSL Research University, Palaiseau, 91120, France
[2]Royal Belgian Institute for Space Aeronomy, Brussels, Belgium
[3]Centre for Atmospheric Chemistry, School of Earth, Atmospheric and Life Sciences, University of Wollongong, Wollongong, Australia
[4]University of Bremen, Bremen, Germany
[5]Max Planck Institute for Biogeochemistry, Jena, Germany
[6]Ludwig-Maximilians-Universität München, Lehrstuhl für Physik der Atmosphäre, Munich, Germany
[7]Deutsches Zentrum für Luft- und Raumfahrt, Institut für Physik der Atmosphäre, Oberpfaffenhofen, Germany
[8]Izaña Atmospheric Research Center (IARC), State Meteorological Agency of Spain (AEMET), Spain
[9]Karlsruhe Institute of Technology (KIT), Institute of Meteorology and Climate Research (IMK-ASF), Karlsruhe, Germany
[10]NASA Ames Research Center, Moffett Field, CA, USA
[11]Finnish Meteorological Institute, Sodankylä, Finland
[12]National Institute for Environmental Studies (NIES), Tsukuba, Japan
[13]National Institute of Water and Atmospheric Research Ltd (NIWA), Lauder, New Zealand
[14]Division of Geological and Planetary Sciences, California Institute of Technology, Pasadena, CA, USA
[15]Japan Aerospace Exploration Agency (JAXA), Tsukuba, Japan
[16]Department of Physics, University of Toronto, Toronto, Canada
[17]Laboratoire d'Etudes du Rayonnement et de la Matière en Astrophysique et Atmosphères (LERMA-IPSL), Sorbonne Université, CNRS, Observatoire de Paris, PSL Université, 75005 Paris, France

Correspondence to: Matthieu Dogniaux (matthieu.dogniaux@lmd.ipsl.fr)

Abstract. A better understanding of greenhouse gas surface sources and sinks is required in order to address the global challenge of climate change. Spaceborne remote estimations of greenhouse gas atmospheric concentrations can offer the global coverage that is necessary to improve the constraint on their fluxes, thus enabling a better monitoring of anthropogenic emissions. In this work, we introduce the Adaptable 4A Inversion (5AI) inverse scheme that aims to retrieve geophysical parameters from any remote sensing observation. The algorithm is based on Bayesian optimal estimation relying on the Operational version of the Automatized Atmospheric Absorption Atlas (4A/OP) radiative transfer forward model along with the Gestion et Étude des Informations Spectroscopiques Atmosphériques: Management and Study of Atmospheric Spectroscopic Information (GEISA) spectroscopic database. Here, the 5AI scheme is applied to retrieve the column-averaged dry-air mole fraction of carbon dioxide (X_{CO_2}) from measurements performed by the Orbiting Carbon Observatory-2 (OCO-2) mission, and uses an empirically corrected absorption continuum in the O_2 A-band. For airmasses

https://doi.org/10.5194/amt-2020-403
Preprint. Discussion started: 10 November 2020

below 3.0, X_{CO_2} retrievals successfully capture the latitudinal variations of CO_2, as well as its seasonal cycle and long-term increasing trend. Comparison with ground-based observations from the Total Carbon Column Observing Network (TCCON) yields a difference of 1.33 ± 1.29 ppm, which is similar to the standard deviation of the Atmospheric CO_2 Observations from Space (ACOS) official products. We show that the systematic differences between 5AI and ACOS results can be fully removed by adding an average 'calculated – observed' spectral residual correction to OCO-2 measurements, thus underlying the critical sensitivity of retrieval results to forward modelling. These comparisons show the reliability of 5AI as a Bayesian optimal estimation implementation that is easily adaptable to any instrument designed to retrieve column-averaged dry-air mole fractions of greenhouse gases.

1. Introduction

The atmospheric concentration of carbon dioxide (CO_2) has been rising for decades because of fossil fuel emissions as well as land-use changes, and large uncertainties still remain in the global carbon budget (e.g. Le Quéré et al., 2009). In order to address the global challenge of climate change, a better understanding of carbon sources and sinks is necessary and remote spaceborne estimations of CO_2 columns can help constraining these carbon fluxes in atmospheric inversion studies, and thus reducing the remaining uncertainties (e.g. Rayner and O'Brien, 2001; Chevallier et al., 2007; Basu et al., 2013, 2018).

The column-averaged dry-air mole fraction of CO_2 (X_{CO_2}) can be retrieved from thermal infrared (TIR) soundings, mostly sensitive to the mid-troposphere (e.g. Chédin et al., 2003; Crevoisier et al., 2004, 2009a), as well as from near-infrared (NIR) and shortwave infrared (SWIR) measurements, which are sensitive to the whole atmospheric column, and especially to levels close to the surface, where carbon fluxes take place. The Scanning Imaging Absorption Spectrometer for Atmospheric Chartography (SCIAMACHY) (Bovensmann et al., 1999) mission provided the first retrievals of X_{CO_2} from NIR and SWIR measurements with the Weighting Function Modified Differential Optical Absorption Spectroscopy (WFM-DOAS) least-squares algorithm (Buchwitz et al., 2005). Bayesian Optimal Estimation, assuming a priori state and covariance for the atmospheric parameters (Rodgers, 2000), was preferred for the more recent X_{CO_2} retrieval algorithm Bremen Optimal Estimation DOAS (BESD) dedicated to SCIAMACHY (Reuter et al., 2010, 2011). Current NIR and SWIR satellite missions observing greenhouse gases include the Japanese Greenhouse gases Observing SATellites (GOSAT and GOSAT-2), NASA's Orbiting Carbon Observatory-2 and 3 (OCO-2 and OCO-3), the Chinese mission TanSat and Sentinel 5-Precursor from the European Space Agency (ESA). Over time, different algorithms based on various assumptions have been developed to exploit their measurements and retrieve greenhouse gas concentrations. Those include the Japanese National Institute for Environmental Studies (NIES) algorithm (Yokota et al., 2009; Yoshida et al., 2011, 2013), as well as the Atmospheric CO_2 Observations from Space (ACOS) algorithm (Bösch et al., 2006; Connor et al., 2008; O'Dell et al., 2012, 2018), UoL-FP from the University of Leicester (Parker et al., 2011), RemoTeC from the Netherlands Institute for Space Research (SRON)

https://doi.org/10.5194/amt-2020-403
Preprint. Discussion started: 10 November 2020

(Butz et al., 2011; Wu et al., 2018) and the Fast atmOspheric traCe gAs retrievaL (FOCAL) algorithm from the University of Bremen (Reuter et al., 2017a, 2017b).

Besides implementing different inverse methods, these algorithms also rely on different forward radiative transfer models to compute synthetic measurements and their partial derivatives. WFM-DOAS and BESD use SCIATRAN (Rozanov et al., 2002, 2014) with the time-efficient correlated-k approximation (Buchwitz et al., 2000), and take into account multiple scattering. The X_{CO_2} retrievals performed by NIES (Yoshida et al., 2011) use a fast radiative transfer model that uses the k-space to increase computational speed for multiple scattering (Duan et al., 2005). RemoTeC uses LINTRAN v2.0, which is a linearized vector (handling the four components of the Stokes vector at the same time) radiative transfer forward model that employs forward-adjoint theory to solve the radiative transfer equation (Hasekamp and Landgraf, 2002; Schepers et al., 2014). The ACOS X_{CO_2} retrieval algorithm and UoL-FP combine, in a piecemeal approach, the LIDORT model to perform a scalar single-scattering radiative transfer computation with the discrete ordinate method (Spurr, 2002) and a second-order-of-scattering polarization model named 2OS (Natraj et al., 2008). FOCAL uses a scalar radiative transfer model that approximates multiple-scattering by assuming the presence of a unique optically thin isotropic scattering layer in the atmosphere, thus enabling fast forward modelling (Reuter et al., 2017a).

These radiative transfer models also fundamentally depend on spectroscopic databases containing the parameters enabling to compute the atmospheric gas absorption. The previously mentioned retrieval algorithms mainly rely on the HITRAN spectroscopic database that evolved over the years: WFM-DOAS uses HITRAN 2008 (Rothman et al., 2009) as does the UoL-FP (with some updated CO_2, H_2O and CH_4 spectroscopic lines). RemoTeC and GOSAT X_{CO_2} retrievals use HITRAN 2008 combined with an O_2 A-band line absorption spectroscopic model taking into account line-mixing and collision-induced absorption (CIA) (Tran and Hartmann, 2008) as well as another line-mixing model for CO_2 lines (Lamouroux et al., 2010). BESD relies on ABSCO v4.0 (computed by ACOS for OCO-2 processing), as does FOCAL for H_2O (Thompson et al., 2012, Reuter et al., 2017a, 2017b). Finally, the ACOS X_{CO_2} retrieval algorithm producing the OCO-2 official product uses ABSCO v5.0 (Drouin et al., 2017; O'Dell et al., 2018; Oyafuso et al., 2017), as does FOCAL, for O_2 and CO_2 (Reuter et al., 2017a).

The design of an X_{CO_2} retrieval algorithm, from the forward model and the spectroscopic parameters it uses to the choice of the adjusted quantities in the state vector, has a critical influence on the overall performance of the observing system (Rodgers, 2000). The systematic errors in retrieved X_{CO_2} and their standard deviations (the latter being also called single measurement precision) with regard to the true (but unknown) state of the atmosphere particularly impact the uncertainty reduction and bias in atmospheric CO_2 flux inversion studies (e.g. Chevallier et al., 2007). However, direct in-situ measurements of CO_2 atmospheric concentration profiles are logistically too difficult to scale up for systematic validation of spaceborne measurements, and so retrieved X_{CO_2} products are most often validated against columns with similar observation geometry, like the ground based solar absorption spectrometry. The Total Carbon Column Observing Network (TCCON) is a network of ground stations that retrieve column-averaged dry-air mole fraction of CO_2 and other species from NIR and SWIR spectra measured with Fourier Transform Spectrometers (FTS) directly pointing at the sun (Wunch et al., 2011b). The network currently consists of 27 stations all around the world and its products constitute a "truth-proxy" reference for the validation of spaceborne retrievals of greenhouse gas atmospheric concentrations. For instance, TCCON datasets were used to validate SCIAMACHY (Reuter et al., 2011), GOSAT X_{CO_2} retrieved by the ACOS (Wunch et al., 2011a) and NIES algorithms (Inoue et al., 2016) and OCO-2 X_{CO_2} produced by ACOS (O'Dell et al., 2018; Wunch et al., 2017), RemoTeC (Wu et al., 2018) and FOCAL (Reuter et al., 2017b). These three last algorithms exhibit different biases with regard to TCCON, depending on their respective forward modelling and bias correction strategies: 0.30 ± 1.04 ppm, 0.0 ± 1.36 ppm and 0.67 ± 1.34 ppm for OCO-2 nadir land soundings, respectively.

In this paper, we present the Adaptable 4A Inversion (5AI) that relies on the OPerational version of the Automatized Atmospheric Absorption Atlas (4A/OP) radiative transfer model (Scott and Chédin, 1981; Tournier, 1995; Cheruy et al., 1995) (https://4aop.aeris-data.fr) and the GEISA (Gestion et Étude des Informations Spectroscopiques Atmosphériques: Management and Study of Spectroscopic Information) spectroscopic database (Jacquinet-Husson et al., 2016) (http://cds-espri.ipsl.fr/etherTypo/?id=950). Here, version 2015 of GEISA is used. The 5AI scheme is applied to retrieve X_{CO_2} from (1) OCO-2 cloud-free target session soundings between 2014 and 2018 and (2) a sample of two years of OCO-2 nadir clear sky measurements with a global land coverage. We compare 5AI retrieval results to TCCON, and to ACOS and FOCAL v08 results over identical sets of soundings in order to assess the reliability of 5AI as a Bayesian optimal estimation implementation.

This paper is organized as follows: Sect. 2 describes the 5AI retrieval scheme and its current features, as well as the 4A/OP radiative transfer model, the GEISA spectroscopic database and the empirically corrected O_2 A-band absorption continuum on which it relies. Section 3 presents the OCO-2 and TCCON data selection. Section 4 presents the a posteriori filters used for this work and shows the 5AI X_{CO_2} target and nadir retrieval results which are compared to TCCON, ACOS and available FOCAL v08 X_{CO_2} products. Section 4 finally underlines the critical importance of forward modelling differences to explain systematic differences between different X_{CO_2} products through an average calculated – observed spectral residual correction. Section 5 highlights the conclusions of this work.

2. The 5AI retrieval scheme

As for any other retrieval scheme, 5AI aims at finding the estimate of atmospheric and surface parameters (for example trace gas concentration, temperature profile, surface albedo, or scattering particle optical depth) that best fits hyperspectral measurements made from space. This inverse problem can be expressed with the following equation:

$$\boldsymbol{y} = F(\boldsymbol{x}) + \boldsymbol{\varepsilon} \quad (1)$$

where $\boldsymbol{y}$ is the measurement vector containing the radiances measured by the space instrument, $\boldsymbol{x}$ is the state vector containing the geophysical parameters to be retrieved, $\boldsymbol{\varepsilon}$ is the measurement noise and finally F is the forward radiative transfer model that describes the physics linking the geophysical parameters to be retrieved to the measured infrared radiances.

2.1 Forward modelling: 4A/OP and GEISA spectroscopic database

The 5AI retrieval scheme uses the OPerational version of the Automatized Atmospheric Absorption Atlas (4A/OP). 4A/OP is an accurate line-by-line radiative transfer model that enables a fast computation of atmospheric transmittances based on atlases containing pre-computed monochromatic optical thicknesses for reference atmospheres. Those are used to compute atmospheric transmittances, for any input atmospheric profile and viewing configuration, that enable to solve the radiative transfer equation and yield radiances and their partial derivatives with regard to the input geophysical parameters at a pseudo-infinite spectral resolution (0.0005 cm^{-1} best) or convolved with an instrument function. 4A/OP is the reference radiative transfer model for the Centre National d'Études Spatiales (CNES) / EUMETSAT IASI Level 1 Calibration/Validation and operational processing, and it is used for daily retrieval of mid-tropospheric columns of CO_2 (Crevoisier et al., 2009a) and CH_4 (Crevoisier et al., 2009b) from the Infrared Atmospheric Sounding Imager (IASI). Moreover, 4A/OP has also been chosen by CNES as the reference radiative transfer model for the development of the New Generation of the IASI instrument (IASI-NG) (Crevoisier et al., 2014).

Although originally developed for the thermal infrared spectral region, 4A/OP now also includes near and shortwave infrared regions (NIR and SWIR). The extension to NIR and SWIR brought important new features to 4A/OP: (1) The computation of the atlases of optical thickness was extended to the 3,000 – 13,500 cm^{-1} domain and takes into account line-mixing and CIA in the O_2 A-band (Tran and Hartmann, 2008) as well as line-mixing and H_2O-broadening of CO_2 lines (Lamouroux et al., 2010). The absorption lines of CO_2 we use in this work are thus identical to those included in HITRAN 2008; (2) Solar spectrum is a flexible input and the Doppler shift of its lines is computed; (3) The radiative transfer model is now coupled with the LIDORT model (Spurr, 2002) for scalar multiple-scattering simulation performed with the discrete ordinates method, as well as with VLIDORT (Spurr, 2006) if polarization or Bidirectional Reflectance Distribution Functions (BRDF) need to be taken into account. These new features are critical for the preparation of the French NIR and

SWIR CO_2 remote sensing MicroCarb mission (Pascal et al., 2017) and the French-German MEthane Remote sensing LIdar Mission (MERLIN) (Ehret et al., 2017).

The 4A/OP radiative transfer model can be used with monochromatic optical thickness atlases computed from any spectroscopic database. For this present work, the atlases are computed using the GEISA 2015 (Gestion et Étude des Informations Spectroscopiques Atmosphériques: Management and Study of Spectroscopic Information) spectroscopic database. Being the base of many work since the beginning in the astronomical and astrophysical communities, GEISA has been also used since the 2000's for the preparation of several current and future spatial missions, as to be chosen by CNES as the reference spectroscopic database for the definition of IASI-NG, MicroCarb and MERLIN. Due to imperfections in the Tran and Hartmann (2008) line mixing and CIA models, an empirical correction to the absorption continuum in the O_2 A-band, fitted from Park Falls TCCON spectra following the method described in Drouin et al. (2017), has been added. Finally, we use Toon (2015) as input solar spectra.

2.2 Inverse modelling in the 5AI retrieval scheme

2.2.1 Bayesian optimal estimation applied for X_{CO_2} retrieval

The whole formalism of Bayesian optimal estimation that enables to find a satisfying solution to Eq. (1) may be found in Rodgers (2000). This subsection only outlines the key steps that are implemented in order to retrieve X_{CO_2}.

Equation (1) includes ε, the experimental noise of the measured radiances. Hence, it appears more appropriate to use a formalism that takes into account this measurement uncertainty and translates it into retrieval uncertainty. Considering the probability density function instead of vectors can bring such an insight. With Gaussian statistics, the inversion problem boils down to the minimization of the following χ^2 cost function:

$$\chi^2 = \left(\boldsymbol{y} - F(\boldsymbol{x})\right)^T \boldsymbol{S_e^{-1}}\left(\boldsymbol{y} - F(\boldsymbol{x})\right) + (\boldsymbol{x} - \boldsymbol{x_a})^T \boldsymbol{S_a^{-1}}(\boldsymbol{x} - \boldsymbol{x_a}) \quad (2)$$

where $\boldsymbol{x_a}$ is the *a priori* state vector, which is also in most cases chosen as the first guess for iterative retrievals. Assuming again Gaussian statistics, $\boldsymbol{S_a}$ is the *a priori* state covariance matrix that represents the variability around the *a priori* state vector, and similarly $\boldsymbol{S_e}$ is the *a priori* measurement error covariance matrix that represents the noise model of the instrument. Moreover, as radiative transfer is a highly non-linear forward model, it is practical to use a local linear approximation, here expressed around the *a priori* state:

$$F(\boldsymbol{x}) = F(\boldsymbol{x_a}) + \frac{\partial F}{\partial x}(\boldsymbol{x_a})(\boldsymbol{x} - \boldsymbol{x_a}) \; . \quad (3)$$

The partial derivatives of the forward radiative transfer model F (here 4A/OP) are expressed as a matrix, called the Jacobian matrix, and denoted $\boldsymbol{K}$.

https://doi.org/10.5194/amt-2020-403
Preprint. Discussion started: 10 November 2020

All these assumptions enable the maximum posterior probability state $\hat{\boldsymbol{x}}$ that minimizes the cost function defined in Eq. (2) to be found. It can be computed by iteration, using the general approach:

$$\boldsymbol{x}_{i+1} = \boldsymbol{x}_i + \left[(1+\gamma)\boldsymbol{S}_a^{-1} + \boldsymbol{K}_i^T\boldsymbol{S}_e^{-1}\boldsymbol{K}_i\right]^{-1}\left(\boldsymbol{K}_i^T\boldsymbol{S}_e^{-1}\left(\boldsymbol{y} - F(\boldsymbol{x}_i)\right) - \boldsymbol{S}_a^{-1}(\boldsymbol{x}_i - \boldsymbol{x}_a)\right) \quad (4)$$

where γ is a scaling factor that can be set to 0 (Gauss-Newton method) or whose value can be adapted along iterations in order to prevent divergence (Levenberg-Marquardt method). $\boldsymbol{K}_i$ denotes here the forward radiative transfer Jacobian matrix, whose values are evaluated for the state vector $\boldsymbol{x}_i$. In this work we assume a slow variation of the Jacobian matrix along the iterations and therefore choose not to update it in order to save computational time. Hence, the partial derivatives of the radiative transfer model are evaluated once and for all around the *a priori* state. We performed a sensitivity test and assessed that this approximation does not significantly change the retrieval results (not shown).

A successful retrieval reduces the *a priori* uncertainty of the state vector described in $\boldsymbol{S}_a$. The *a posteriori* covariance matrix of the retrieved state vector $\hat{\boldsymbol{S}}$, whose diagonal elements give the posterior variance of the retrieved state vector elements, is expressed as

$$\hat{\boldsymbol{S}} = \left[\boldsymbol{S}_a^{-1} + \boldsymbol{K}^T\boldsymbol{S}_e^{-1}\boldsymbol{K}\right]^{-1} \quad . \quad (5)$$

Finally, the sensitivity of the retrieval with regard to the true geophysical state $\boldsymbol{x}_{true}$ is given by the averaging kernel matrix $\boldsymbol{A}$ calculated according to

$$\boldsymbol{A} = \frac{\partial \hat{x}}{\partial x_{true}}(\boldsymbol{x}_a) = \left[\boldsymbol{S}_a^{-1} + \boldsymbol{K}^T\boldsymbol{S}_e^{-1}\boldsymbol{K}\right]^{-1}\boldsymbol{K}^T\boldsymbol{S}_e^{-1}\boldsymbol{K} \ . \quad (6)$$

In most cases, the CO_2 concentration is included in the state vector as a level or layer profile from which X_{CO_2}, the retrieved column-averaged dry-air mole fraction of CO_2, is computed (e.g. O'Dell et al., 2012). If we note $\hat{\boldsymbol{x}}_{\boldsymbol{CO2}}$, the part of the retrieved state vector $\hat{x}$ containing the CO_2 profile, and $\boldsymbol{A}_{\boldsymbol{CO2}}$ and $\hat{\boldsymbol{S}}_{\boldsymbol{CO2}}$, the corresponding square parts of $\boldsymbol{A}$ and $\hat{\boldsymbol{S}}$, we have:

$$X_{CO_2} = \boldsymbol{h}.\hat{\boldsymbol{x}}_{\boldsymbol{CO_2}} \quad (7)$$

$$\sigma_{X_{CO_2}} = \sqrt{\boldsymbol{h}^T\hat{\boldsymbol{S}}_{\boldsymbol{CO_2}}\boldsymbol{h}} \quad (8)$$

$$\left(\boldsymbol{a}_{\boldsymbol{CO_2}}\right)_j = \frac{\partial X_{CO_2}}{\partial x_{true}} = \frac{\left(h^T A_{CO_2}\right)_j}{h_j} \quad (9)$$

where $\boldsymbol{h}$ is the pressure weighting function. $\sigma_{X_{CO_2}}$ denotes the posterior uncertainty of the retrieved X_{CO_2} and $\boldsymbol{a}_{\boldsymbol{CO_2}}$ is the CO_2 column averaging kernel. This profile vector describes the vertical sensitivity of the retrieved column with regard to the true profile: it is essential to characterize retrieval results and to compare them to other products, as shown in Sect. 4.2.

2.2.2 5AI features and retrieval scheme setups for OCO-2

The 5AI retrieval scheme enables the retrieval of multiple geophysical variables from hyperspectral measurements. Those currently include trace gas concentration represented in the state vector as a concentration profile or a profile scaling-factor, global temperature profile offset, surface temperature and pressure, band-wise albedo whose spectral dependence is modelled as a polynomial, and finally scattering particle layer-wise optical depth.

For this work, the iterative scheme is set to the Levenberg-Marquardt method. The state vector includes the main geophysical parameters necessary to retrieve X_{CO_2} and is described in Table 1. The a priori values and their covariance are identical to those used in the ACOS B8r version (O'Dell et al., 2018) in order to ease the retrieval result comparison, as we aim to assess 5AI reliability. However, some elements of the ACOS state vector are not included in this work: scattering particles optical depth (AOD) as we only consider clear-sky soundings, Solar Induced Fluorescence which is not modelled in 4A/OP, surface wind speed (only land retrievals are considered) and Empirical Orthogonal Function (EOF) scaling factors.

Table 1. 5AI state vector composition for OCO-2 retrievals

Variable name	Length	A priori value	A priori uncertainty (1σ)	Notes
H_2O scaling factor	1	1.0	0.5 (same as ACOS)	-
CO_2 layer concentration	19 layers	ACOS a priori	ACOS prior covariance matrix	See prior covariance matrix in (O'Dell et al., 2012)
Surface Pressure	1	ACOS a priori	4.0 hPa (same as ACOS)	-
Temperature profile offset	1	ACOS a priori	5.0 K (same as ACOS)	-
Surface Albedo (order 0 of albedo model)	3 bands	ACOS a priori	1.0 (same as ACOS)	Evaluated at 0.77, 1.615 and 2.06 µm for O_2, CO_2 weak and strong bands, respectively
Surface Albedo Slope (order 1 of albedo model)	3 bands	0.0	1.0 /cm^{-1}	(O'Dell et al., 2018) explains that this uncertainty is 0.0005 /cm^{-1} but B8r data release uses 1.0 /cm^{-1} in the 'apriori_covariance_matrix', in 'RetrievalResults', in Diagnostics files.

4A/OP is used with VLIDORT for O_2 A-band polarized forward computations, and the ACOS Stokes coefficients are applied to yield the final scalar radiances. For CO_2 weak and strong bands, scattering and polarization can be neglected in clear sky conditions, and only the Stokes coefficient 0.5 for the *I* component of the electric field is applied to yield the final scalar radiances.

https://doi.org/10.5194/amt-2020-403
Preprint. Discussion started: 10 November 2020

3. Data

3.1 Data description

The OCO-2 spectrometer measures Earth-reflected near and shortwave infrared (NIR and SWIR) sunlight in three distinct bands: the O_2 A-band (0.7 µm), the weak CO_2 band (1.6 µm) and the strong CO_2 band (2.0 µm). The satellite has three distinct observation modes. The nadir and glint modes are the nominal science observation modes; they constitute the vast majority of OCO-2 measurements. In addition, the target mode of the OCO-2 mission provides data for the validation of the retrievals. During a target session, the satellite tilts and aims at a validation target (most of them are TCCON stations) and scans its whereabouts several times during the overpass. These sessions thus provide with OCO-2 data points closely collocated with validation targets (over areas that can be as small as 0.2° longitude × 0.2° latitude) and registered over a few minutes (Wunch et al., 2017).

OCO-2 high-resolution spectra are analysed by the ACOS team in order to retrieve X_{CO_2} and other geophysical parameters from them. Two different X_{CO_2} values are provided by the ACOS team: raw and posterior bias-corrected X_{CO_2}. Raw X_{CO_2} is the direct output of the ACOS algorithm following the full physics retrieval: its most recent version is distributed within the B8 retrospective (B8r) ACOS data release (O'Dell et al., 2018). Posterior bias-corrected X_{CO_2} is an empirically corrected X_{CO_2} that has reduced averaged bias with regard to different "truth-proxies" (O'Dell et al., 2018). The last available version of this product is distributed within the B9 retrospective (B9r) ACOS data release. It corrects the impacts of footprint geolocation errors and erroneous prior surface pressure temporal sampling directly in the bias correction procedure applied to the B8r raw X_{CO_2} product, without a complete full-physics reprocessing of all OCO-2 data (Kiel et al., 2019). In this work, 5AI results are compared with B8r raw X_{CO_2}, and B9r posterior bias-corrected X_{CO_2} are also shown.

In addition to ACOS products, we also compare our results with OCO-2 FOCAL v08 data produced at the University of Bremen with the FOCAL algorithm (Reuter et al., 2017a) that includes an empirical posterior bias correction directly on the top of the full-physics retrieval (Reuter et al., 2017b). Only the posterior bias-corrected X_{CO_2} is included in FOCAL v08 data.

In this work, we compare X_{CO_2} retrieved from OCO-2 spectra to TCCON data. The TCCON network uses ground-based high resolution Fourier Transform Spectrometers to measure NIR and SWIR spectra that enable the retrieval of the column-averaged dry-air mole fractions of greenhouse gases. These retrievals are performed by GGG2014 (Wunch et al., 2015) and their results are available on the TCCON Data Archive (https://tccondata.org/).

3.2 Data selection

We intend to compare 5AI results with regard to TCCON against ACOS and FOCAL results for corresponding sets of soundings. First, we select all the OCO-2 target soundings between 2015 and 2018 with low ACOS retrieved total AOD (<0.5) and ACOS cloud, sounding quality and outcome flags at their best possible value. As FOCAL v08 uses prior and posterior filtering techniques that are different from ACOS, only a fraction of this first selection intersects with available FOCAL data. In order to increase this fraction, we add all OCO-2 points with the best ACOS cloud and sounding quality flags intersecting the available FOCAL v08 data points, whatever ACOS outcome flag and retrieved AOD. This composite sample set includes 48,885 OCO-2 target soundings and the fraction of available intersecting FOCAL data is shown in Fig. 1.

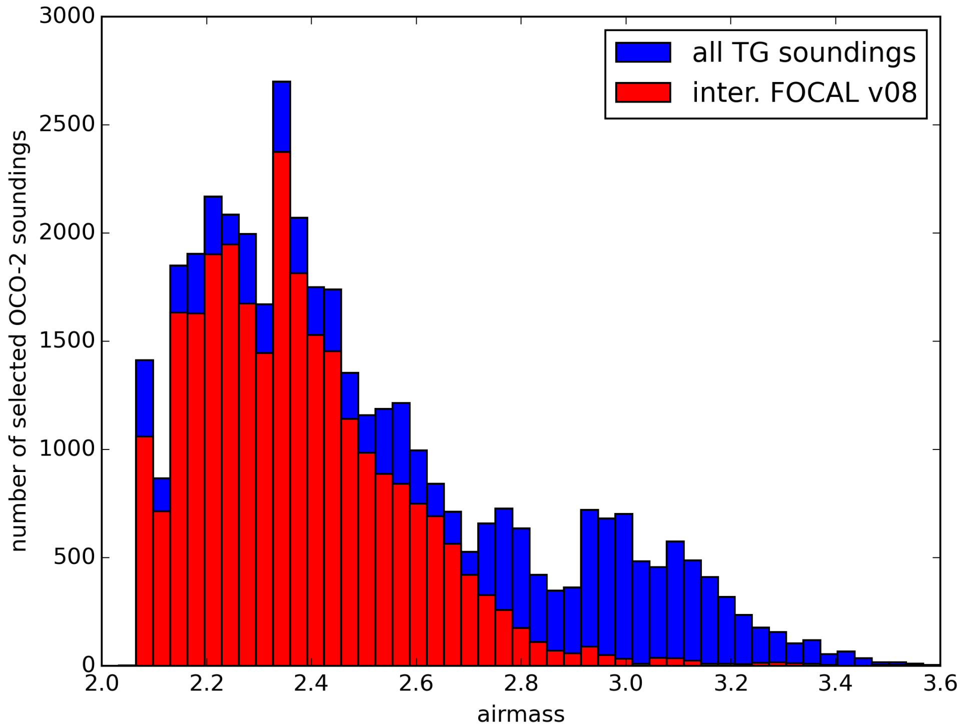

Figure 1. Airmass distributions of all the selected OCO-2 target soundings (blue) and of those intersecting available FOCAL v08 data (red).

https://doi.org/10.5194/amt-2020-403
Preprint. Discussion started: 10 November 2020

For this study, we select the TCCON official products measured ± 2 hours with regard to OCO-2 overpass time and only keep the target sessions where at least five OCO-2 measurements passing 5AI posterior filters and five TCCON data points are available. This set includes 11,102 TCCON individual retrieval results from 20 TCCON stations listed in Table 2.

Table 2. TCCON data used in this work

TCCON station	Coordinates (latitude, longitude, altitude)	Number of target sessions	Date range (first and last sessions)	Reference
Ascension Island	7.92S, 14.33W, 0.01 km	4	2015-01-16 – 2018-01-15	(Feist et al., 2014)
Bialystok (Poland)	53.23N, 23.03E, 0.18 km	1	2015-03-18	(Deutscher et al., 2019)
Bremen (Germany)	53.10N, 8.85E, 0.027 km	1	2016-03-17	(Notholt et al., 2014)
Burgos (Philippines)	18.53N, 120.65E, 0.035 km	2	2017-04-21 – 2018-03-07	(Morino et al., 2018a)
Caltech (USA)	34.14N, 118.13W, 0.230 km	21	2014-09-12 – 2018-09-16	(Wennberg et al., 2015)
Darwin (Australia)	12.424S, 130.89E, 0.03 km	8	2015-05-15 – 2017-07-28	(Griffith et al., 2014a)
Edwards (USA)	34.96N, 117.88W, 0.700 km	3	2015-07-04 – 2018-08-22	(Iraci et al., 2016)
Eureka (Canada)	80.05N, 86.42W, 0.61 km	2	2015-06-16 – 2015-06-28	(Strong et al., 2019)
Izana (Tenerife)	28.31N, 16.50W, 2.37 km	2	2018-01-05 – 2018-03-24	(Blumenstock et al., 2017)
Karlsruhe (Germany)	49.10N, 8.44E, 0.116 km	3	2016-05-07 – 2017-07-06	(Hase et al., 2015)
Lamont (USA)	36.60N, 97.49W, 0.32 km	12	2015-02-10 – 2016-11-11	(Wennberg et al., 2016)
Lauder (New Zealand)	45.04S, 169.68E, 0.37 km	4	2015-02-17 – 2017-01-30	(Sherlock et al., 2014)
Orléans (France)	47.97N, 2.11E, 0.13 km	2	2015-04-08 –	(Warneke et al., 2019)

https://doi.org/10.5194/amt-2020-403
Preprint. Discussion started: 10 November 2020

Atmospheric Measurement Techniques Discussions

			2018-06-26	
Paris (France)	48.85N, 2.36E, 0.06 km	1	2016-08-25	(Té et al., 2014)
Park Falls (USA)	45.95N, 90.27W, 0.44 km	7	2014-10-11 – 2017-04-21	(Wennberg et al., 2017)
Réunion Island	20.90S, 55.49E, 0.087 km	4	2015-03-24 – 2015-08-01	(De Mazière et al., 2017)
Saga (Japan)	33.24N, 130.29E, 0.007 km	6	2015-07-31 – 2018-03-10	(Kawakami et al., 2014)
Sodankylä (Finland)	67.37N, 26.63E, 0.188 km	4	2015-08-20 – 2018-07-17	(Kivi et al., 2014; Kivi and Heikkinen, 2016)
Tsukuba (Japan)	36.05N, 140.12E, 0.03 km	6	2014-11-14 – 2017-06-17	(Morino et al., 2018b)
Wollongong (Australia)	34.40S, 150.88E, 0.03 km	13	2014-09-23 – 2018-05-06	(Griffith et al., 2014b)

Besides target sessions, we also select a sample of clear sky OCO-2 nadir land soundings with a coverage as global as possible over the years 2016-2017 (all ACOS flags at their best value possible). For every month and 5° longitude × 5° latitude bins we select 25 (10 for North-America, South-Africa and Australia) soundings with low ACOS retrieved total AOD. For 2016 and 2017, this selection is done for a maximum ACOS retrieved total AOD of 0.035 and 0.045, respectively, yielding 17,069 soundings for 2016 and 11,002 for 2017. Figure 2 shows the spatial and temporal distribution of these OCO-2 points.

https://doi.org/10.5194/amt-2020-403
Preprint. Discussion started: 10 November 2020

Atmospheric Measurement Techniques Discussions

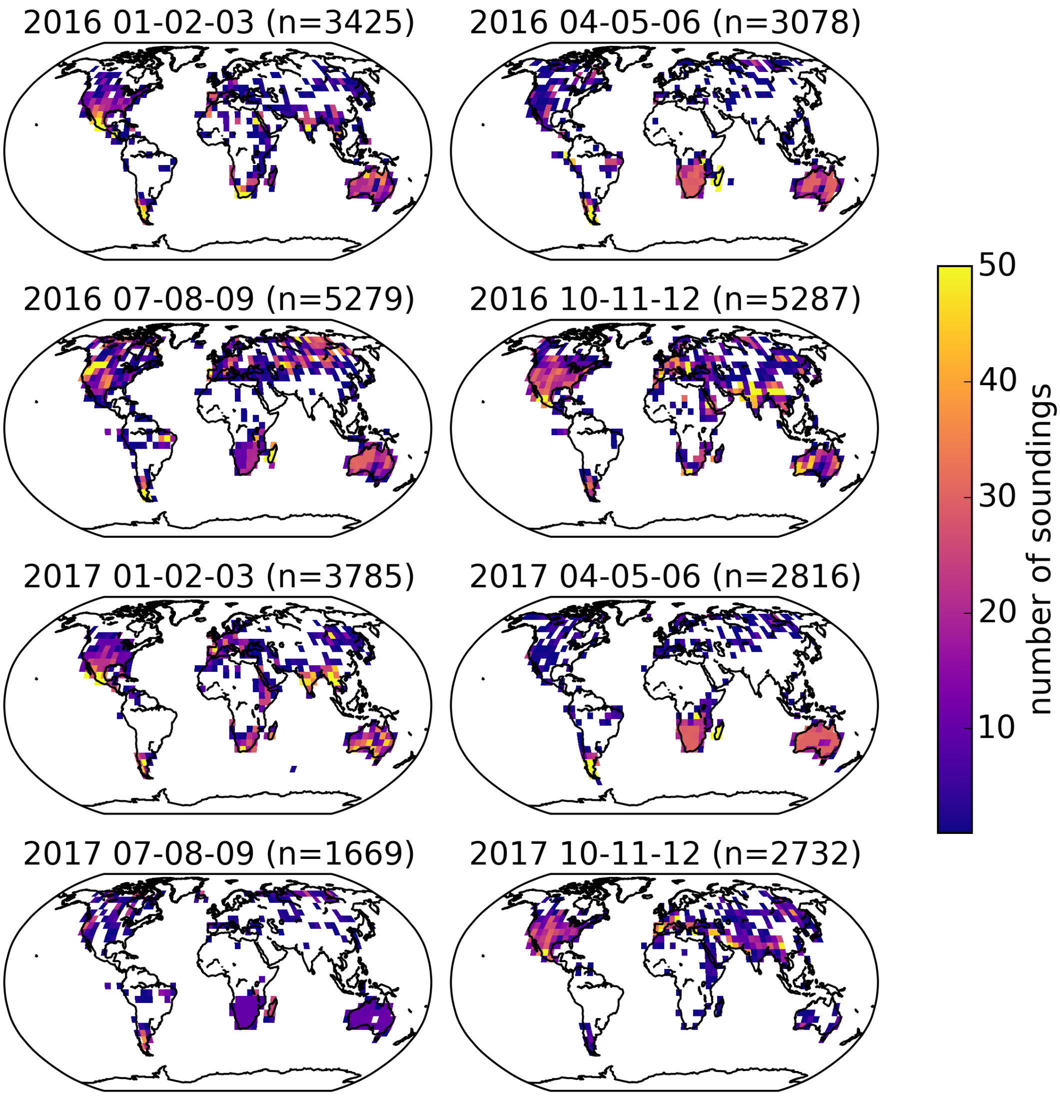

295 **Figure 2. Spatial and temporal repartition of the sample of nadir OCO-2 soundings selected for 5AI retrievals, in seasonal and 5° × 5° square bins. The titles include the number of soundings n for the corresponding panel: the low number of selected soundings in July-August-September 2017 is due to an identified OCO-2 data gap.**

4. Results and discussion

300 ### 4.1 Post-filtering of retrieval results

We apply the a posteriori filters described in Table 3 to ensure retrieval results' quality. The surface pressure filter removes soundings for which it proved difficult to successfully model the optical path, suggesting scattering related errors leading to a large difference between the retrieved and prior surface pressure. The reduced χ^2 filter removes the worst spectral fits. In the end, 88% of our selected soundings pass these first two filters. In addition, the blended albedo filter removes the fraction of target data (29%) representative of challenging snow or ice-covered surfaces (Wunch et al., 2011a). With the current retrieval setup, the difference between the 5AI retrieved surface pressure and its prior exhibit an airmass dependence as shown in Fig. 3. For this present work, we filter out all sounding with airmasses above 3.0. Future studies will refine the 5AI forward and inverse setup in order to process hyperspectral infrared soundings with larger airmasses. Results detailed in the following subsections are based on the 24,449 target and 21,254 nadir OCO-2 soundings that passed all these filters.

Table 3. Filters applied on 5AI retrieval results for this work.

Variable name	Minimum value	Maximum value	Definition and reference	OCO-2 mode
Retrieved surface pressure	P_{nlev-1}	-	The atmosphere is discretized in 20 levels bounding 19 layers. We do not allow the surface pressure, P_{nlev}, to be lower than its preceding pressure level.	Nadir, Target
Reduced χ^2	-	7.0	Overall goodness of the spectral fit (e.g. Wu et al., 2018)	Nadir, Target
Blended albedo	-	0.8	2.4 x O_2 A-band albedo + 1.13 x CO_2 strong band albedo (Wunch et al., 2011a, 2017)	Target
Airmass	-	3.0	$\frac{1}{\cos(SZA)} + \frac{1}{\cos(VZA)}$, with SZA, the solar zenith angle, and VZA, the viewing zenith angle (Wunch et al., 2011a)	Nadir, Target

https://doi.org/10.5194/amt-2020-403
Preprint. Discussion started: 10 November 2020

Atmospheric Measurement Techniques Discussions

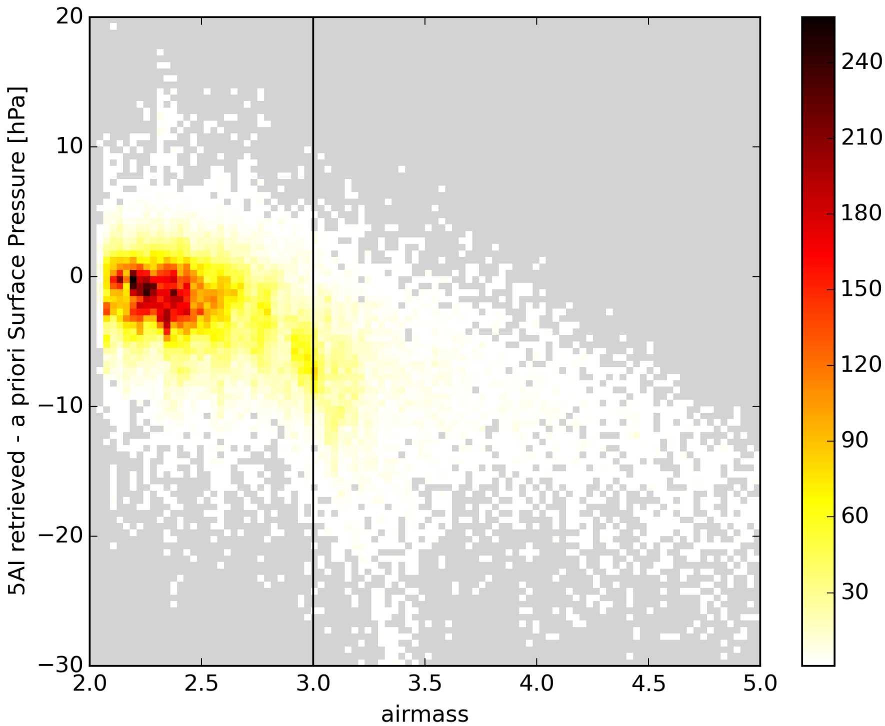

315 **Figure 3. Distribution of target and nadir 5AI retrievals passing surface pressure, blended albedo and reduced $\chi_r{}^2$ filters according to airmass and difference between retrieved and prior surface pressures. Grey areas denote bins for which no 5AI retrieval is available.**

4.2 OCO-2 target retrieval results

For every target session, we consider a unique average of the available retrieval results from OCO-2 measurements and a unique average of the corresponding TCCON official products as performed in e.g. O'Dell et al. (2018) and Wu et al.
320 (2018). As OCO-2 and TCCON X_{CO_2} vertical sensitivities described by their averaging kernels are not exactly identical, we take into account the averaging kernel correction of TCCON data as performed by the ACOS team (O'Dell et al., 2018) and described by Eq. (10) (Nguyen et al., 2014):

$$X_{OCO-2,TCCON} = X_{a\,priori} + \left(\frac{\hat{X}_{TCCON}}{X_{a\,priori}} - 1\right) \sum_j \boldsymbol{h_j} \left(\boldsymbol{a_{CO_2}}\right)_j \boldsymbol{x_{a\,priori,j}} \,. \quad (10)$$

https://doi.org/10.5194/amt-2020-403
Preprint. Discussion started: 10 November 2020

$X_{OCO-2,TCCON}$ is the column-averaged dry-air mole fraction of CO_2 that would have been retrieved from the OCO-2 measurement if the collocated TCCON retrieval was the true state of the atmosphere, $X_{a\,priori}$, the a priori column-averaged dry-air mole fraction of CO_2, considered to be very similar between 5AI (or ACOS) and GGG2014, $\hat{X}_{TCCON}$, the TCCON retrieved column-averaged dry-air mole fraction of CO_2, $\boldsymbol{h}$, the pressure weighting function vector defined previously, $(\boldsymbol{a_{CO_2}})$, the CO_2 column averaging kernel vector defined in Eq. (9) and $\boldsymbol{x_{a\,priori}}$, the a priori CO_2 concentration profile vector. The effect of this correction yields a positive shift of the bias with regard to TCCON of about 0.2 ppm for the set of target sessions considered in this work.

Following post-filtering, Fig. 4 shows 5AI raw results compared to the TCCON official product over 106 target sessions. The mean systematic X_{CO_2} bias (5AI − TCCON) is 1.33 ppm and its standard deviation is 1.29 ppm. The ACOS raw X_{CO_2} and TCCON X_{CO_2} comparison for the corresponding set of OCO-2 soundings is also presented in Fig. 4: the bias with regard to TCCON is -2.08 ppm and its standard deviation is 1.27 ppm. This difference in bias compared to TCCON may be greatly influenced by forward modelling differences between 5AI and ACOS, as detailed later in this work. Bias-corrected RemoTeC X_{CO_2} retrieval results compared to the ACOS official product exhibit similar differences in bias standard deviations (Wu et al., 2018).

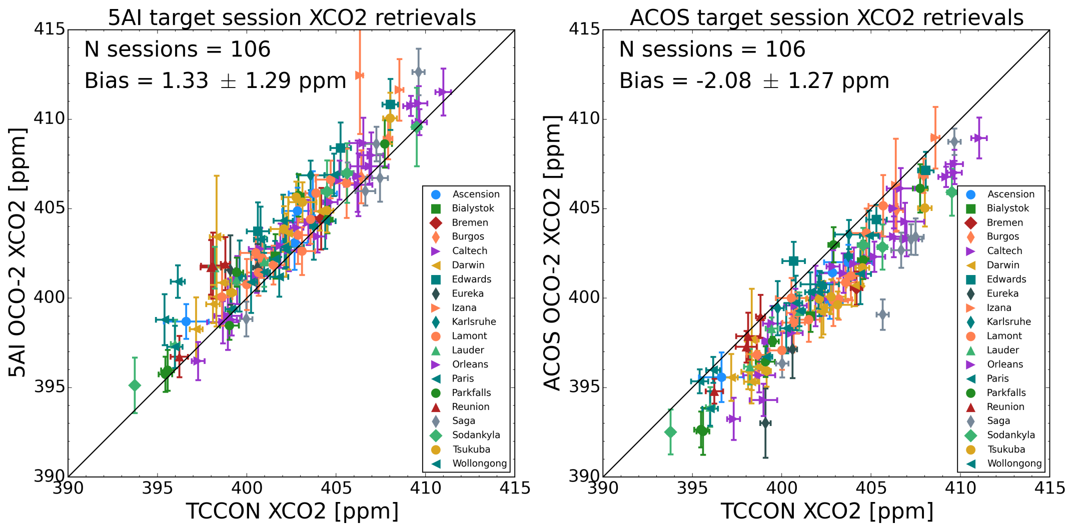

Figure 4. 5AI (left) and raw ACOS B8r (right) OCO-2 target X_{CO_2} retrieval results compared to TCCON official X_{CO_2} product. Individual sounding results are averaged for every target session: markers show session average for OCO-2 and TCCON X_{CO_2}, and error bars show standard deviations.

https://doi.org/10.5194/amt-2020-403
Preprint. Discussion started: 10 November 2020

Atmospheric Measurement Techniques
Discussions

Temporal and latitudinal fits of 5AI and ACOS X_{CO_2} biases compared to TCCON are displayed in Fig. 5. Temporal biases are fitted with a 1st order polynomial added to a cosine and exhibit quasi-null slope with a ~0.4 ppm amplitude of yearly oscillation in both 5AI and ACOS cases. Latitudinal bias fits performed with all the available target sessions except those from Eureka (full lines) show that 5AI bias compared to TCCON appears to be larger in the Southern hemisphere than in the Northern hemisphere, but its behaviour is quite parallel to ACOS except at higher latitudes where 5AI and ACOS get closer. The Eureka station (latitude 80°N) has been removed from those fits as satellite retrievals and validation are known to be challenging at these latitudes (O'Dell et al., 2018). The same latitudinal bias fits performed on the dataset intersecting available FOCAL v08 data (dashed lines) show improved 5AI bias compared to TCCON. This is mainly due to the airmass distribution difference between the two sets displayed in Fig. 1.

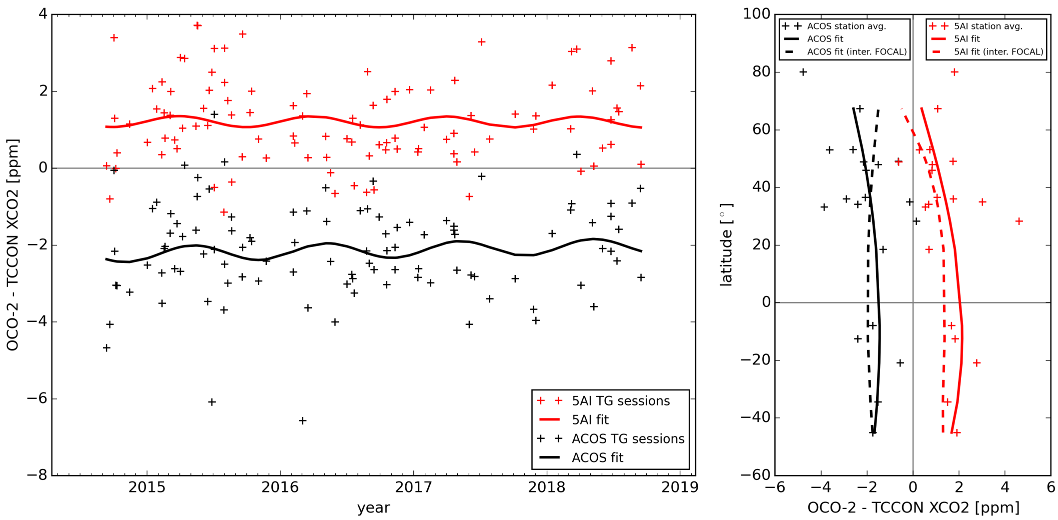

Figure 5. 5AI and raw ACOS B8r OCO-2 target X_{CO_2} bias with regard to TCCON as a function of time (left panel) and latitude (right panel). Crosses show individual session averages in the left panel and individual station averages in the right panel, full lines show polynomial fits of this bias for all target sessions, and dashed lines represent the polynomial fits of this bias for the target sessions intersecting FOCAL v08 available soundings, used for the simplistic empirical bias correction applied in Fig. 6.

Finally, a consistent comparison of 5AI, ACOS and FOCAL v08 on this intersecting set of available soundings is performed in Fig. 6. Its first column shows 5AI and ACOS raw X_{CO_2} results. As previously mentioned, FOCAL v08 only distributes a posterior bias-corrected X_{CO_2} product. Thus, in order to provide a more consistent comparison of the three retrieval schemes, in the second column of Fig. 6, we apply a simplistic empirical correction on 5AI and ACOS results that removes the fitted latitudinal bias with regard to TCCON, presented in dashed lines in the right panel of Fig. 5. Finally, the last column of Fig.

https://doi.org/10.5194/amt-2020-403
Preprint. Discussion started: 10 November 2020

Atmospheric Measurement Techniques Discussions
Open Access
EGU

6 shows official posterior bias-corrected ACOS B9r and FOCAL v08 products. The standard deviations of these biases are quite similar between the three retrieval schemes (0.05 ppm difference between 5AI and ACOS, 0.01 ppm difference between 5AI and FOCAL v08). The slight improvement of 5AI bias compared to TCCON between Fig. 4 and Fig. 6 is due to the differences in airmass distribution between the two sounding sets.

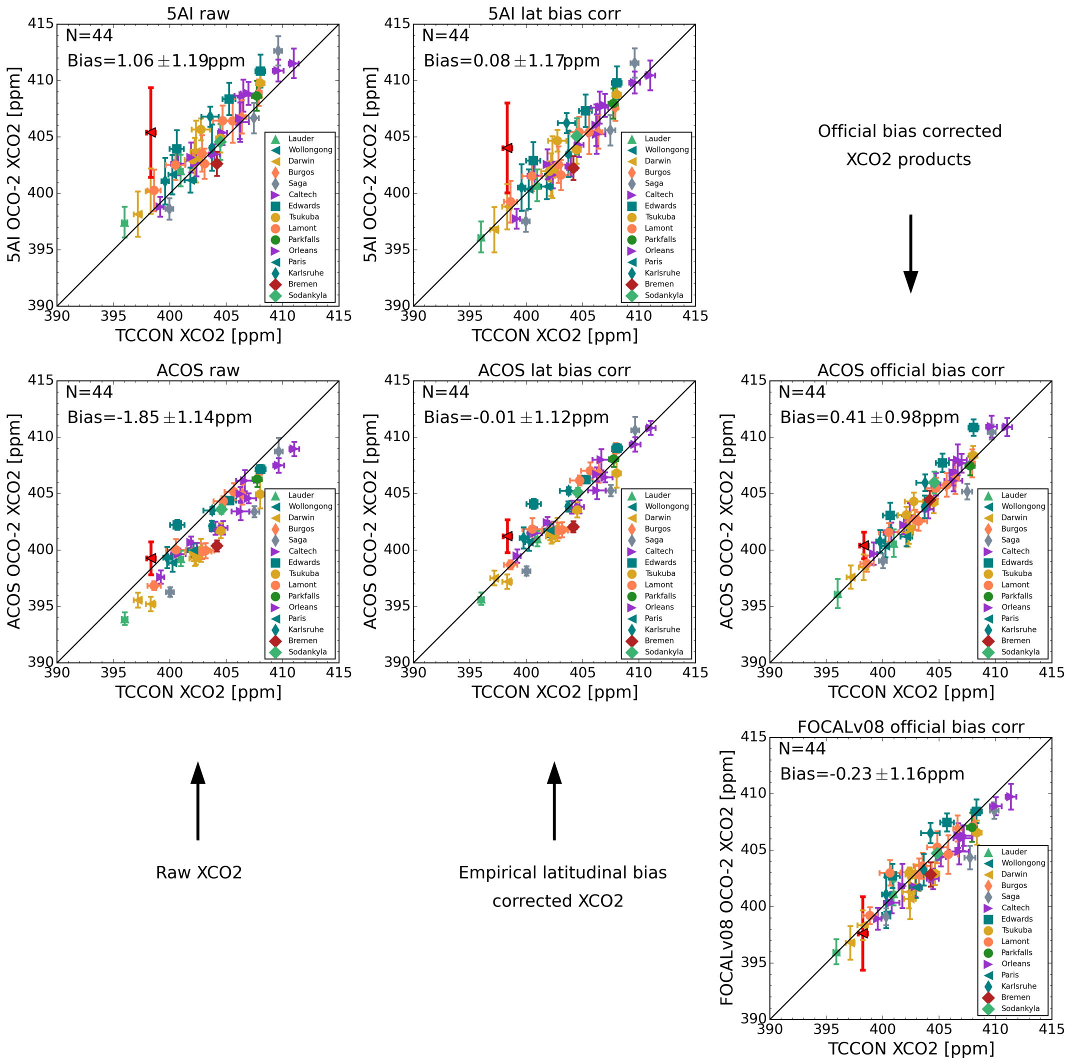

Figure 6. 5AI (top row panels), ACOS B8r for raw products and B9r for the official bias-corrected one (center row panels) and

https://doi.org/10.5194/amt-2020-403
Preprint. Discussion started: 10 November 2020

FOCAL v08 (bottom row panel) OCO-2 target X_{CO_2} retrieval results compared to TCCON official X_{CO_2} product. Depending on data availability, we show raw X_{CO_2} results (left column panels), simplistically corrected X_{CO_2} results based on a latitudinal bias fit (central column panels) and official bias-corrected X_{CO_2} products (right column panels). Individual sounding results are averaged for every target session: markers show session average for OCO-2 and TCCON X_{CO_2}, and error bars show standard deviations. One target session in Darwin on the 11th of September 2015 distinguishes itself from other sessions with either increased bias compared to TCCON or OCO-2 session-wise standard deviation for the three algorithms. It has been manually removed from the statistics but still appears in red with black lining in the figure.

4.3 OCO-2 nadir retrieval results

In this subsection, raw 5AI retrieved X_{CO_2} is compared to the ACOS raw product on a sample of OCO-2 nadir clear sky soundings as described in Sect. 3 and displayed in Fig. 2. The nadir viewing configuration is the nominal science mode of the OCO-2 mission and allows comparisons at a larger spatial scale than the one offered by the target mode dedicated to validation.

Figure 7 shows the average and associated standard deviation of the difference between 5AI and ACOS retrieved raw X_{CO_2}. The overall 5AI-ACOS difference is about 3 ppm, with a latitudinal dependency: it is lower above mid-latitudes in the Northern hemisphere. The standard deviation is mainly correlated with topography: it is higher in the vicinity of mountain chains and lower on flatter areas. As we do not take into account topography in the sampling strategy of the processed OCO-2 nadir soundings, its greater variability in mountainous areas can result in a greater variability of the retrieved surface pressure which is strongly correlated with retrieved X_{CO_2}. As for the highest standard deviations in South America, they may be caused by the South Atlantic Anomaly to which they are close (Crisp et al., 2017).

https://doi.org/10.5194/amt-2020-403
Preprint. Discussion started: 10 November 2020

Atmospheric Measurement Techniques
Discussions

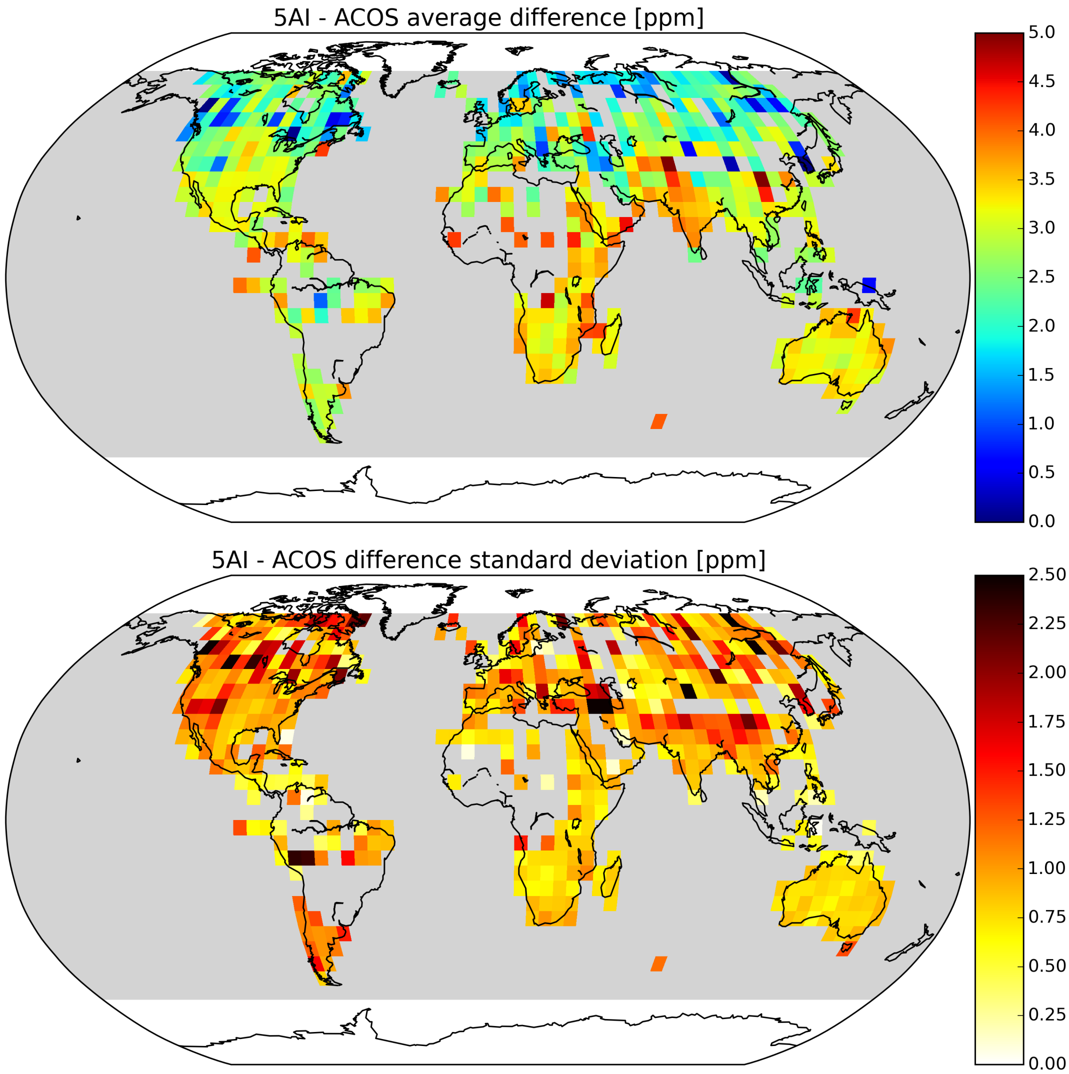

Figure 7. Spatial repartition of 5AI – raw ACOS B8r average difference and its standard deviation on 5° × 5° square bins for the nadir data selection.

395

https://doi.org/10.5194/amt-2020-403
Preprint. Discussion started: 10 November 2020

As seen in Fig. 8, latitudinal variations of raw 5AI retrieved X_{CO_2} are consistent with those of ACOS, with a difference between the two products almost constant except above mid-latitudes in the Northern hemisphere where the differences are smaller. In addition, the comparison between 5AI and ACOS in nadir mode is consistent with the results obtained for target sessions. Indeed, the raw 5AI – ACOS target difference lies within $\pm$ 1 σ of nadir results, with σ the standard deviation of the 5AI – ACOS difference. Figure 9 details the temporal variations of the retrieved X_{CO_2}. The global long-term increase of the atmospheric concentration of CO_2 can be observed in both hemispheres as well as the seasonal cycle, stronger in the Northern hemisphere where most of the vegetation respiration and photosynthesis happen. The temporal variations of the 5AI – ACOS X_{CO_2} retrieval differences in nadir mode are also consistent with those presented in target mode.

https://doi.org/10.5194/amt-2020-403
Preprint. Discussion started: 10 November 2020

Atmospheric Measurement Techniques
Discussions

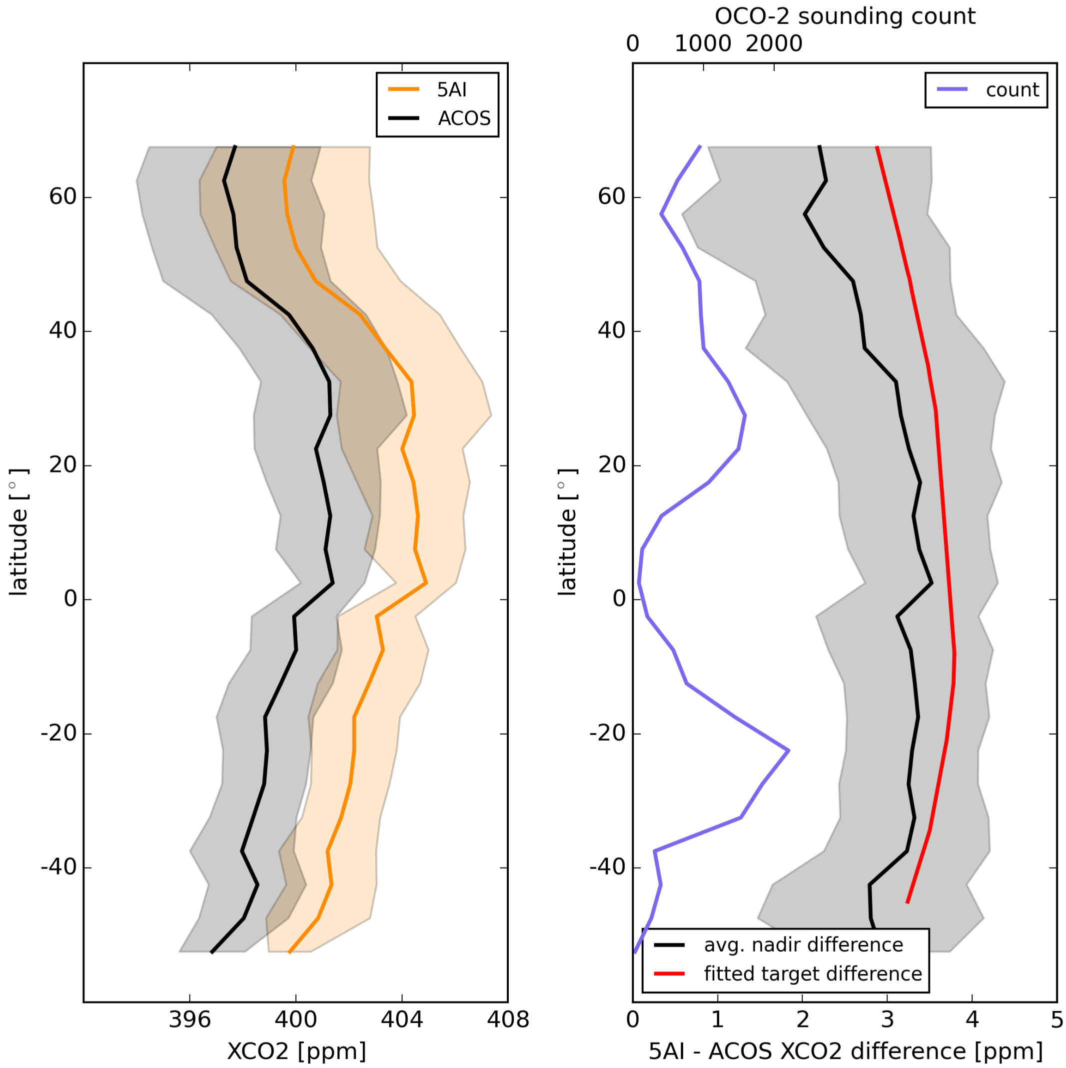

405 **Figure 8. Latitudinal variation of 5AI and raw ACOS B8r retrieved X_{CO_2} (left) and their difference (right). The right panel compares 5AI-ACOS average difference for nadir soundings and 5AI-ACOS difference fitted on target sessions (bottom axis). The number of available nadir soundings is also shown in the right panel (top axis).**

https://doi.org/10.5194/amt-2020-403
Preprint. Discussion started: 10 November 2020

Atmospheric Measurement Techniques
Discussions

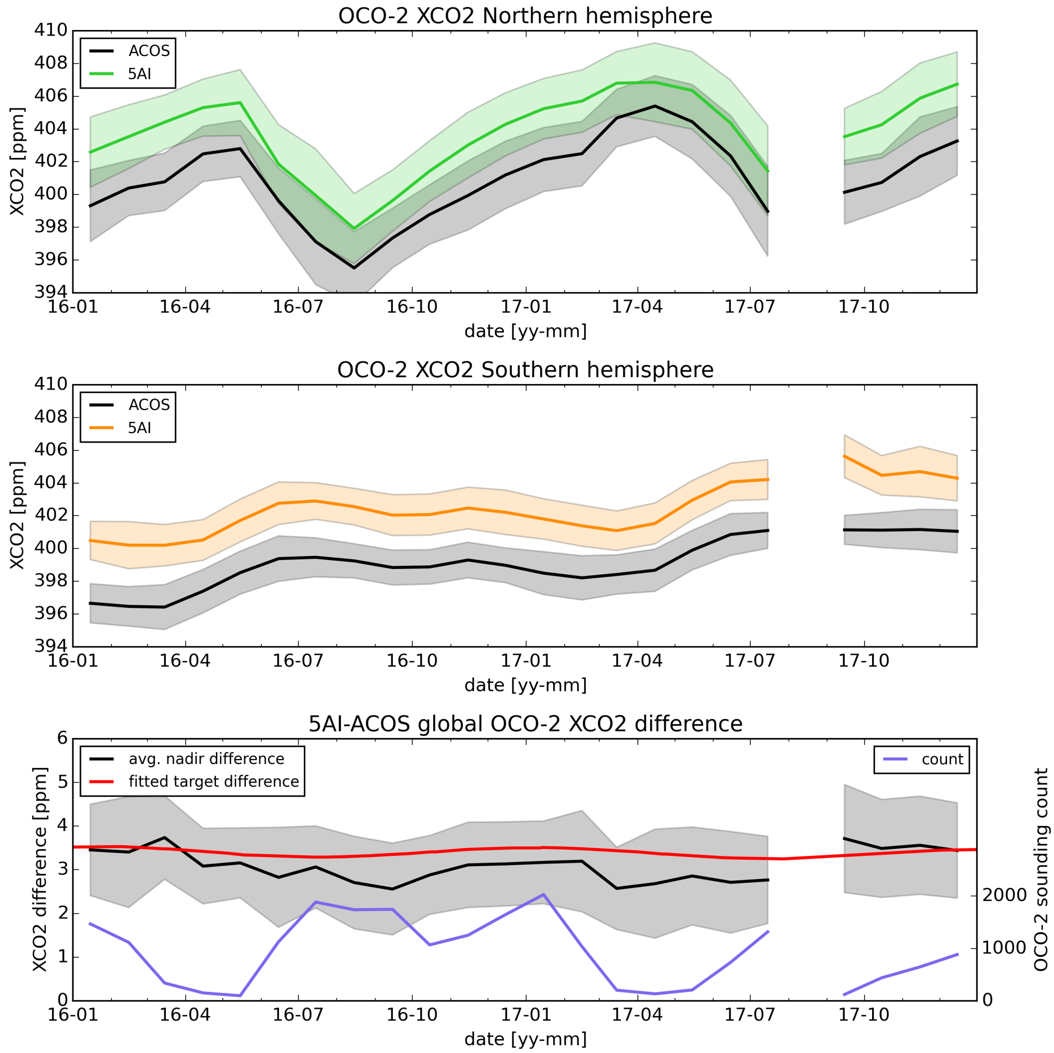

410 **Figure 9. Temporal variation of 5AI and raw ACOS B8r retrieved X_{CO_2} in the Northern hemisphere (top), Southern hemisphere (center) and the global difference (bottom). The bottom panel compares 5AI-ACOS difference for nadir and target OCO-2.**

https://doi.org/10.5194/amt-2020-403
Preprint. Discussion started: 10 November 2020

Atmospheric Measurement Techniques Discussions

4.4 Sensitivity of raw retrieval results to forward modelling

A difference of about 3 ppm is found between 5AI and ACOS raw X_{CO_2} retrieved from OCO-2 for both nadir and target observations. As mentioned in Sect. 1 and 2, 5AI and ACOS retrieval schemes rely on different radiative transfer models and spectroscopic inputs, and their respective retrieval setups are also quite different. In order to quantify the impact of these differences, we perform an average 'calculated – observed' spectral residual analysis (hereafter 'calc – obs'), where the calculated spectrum (convolved to OCO-2 Instrument Line Shape) is generated by the forward model 4A/OP using GEISA spectroscopic database and the ACOS retrieval results (posterior pressure grid, temperature, H_2O and CO_2 profiles as well as albedo and albedo slope), and is compared to the corresponding OCO-2 observation. In addition, possible background differences are compensated by scaling the OCO-2 spectrum so that its transparent spectral windows fit those of the 4A/OP calculated spectrum. This comparison is performed for a randomly chosen half of the nadir OCO-2 points with an airmass below 3.0 selected in 2016 (6,790 in total). Figure 10 shows the resulting averaged calculated – observed spectral residuals as well as the typical transmission of the OCO-2 measurements. Differences are principally located in the 0.7 µm O_2 absorption band, but also in the 1.6 and 2.0 µm CO_2 absorption bands. They are due to the radiative transfer models' differences between ACOS and 5AI (parametrization of continua, spectroscopy, etc).

https://doi.org/10.5194/amt-2020-403
Preprint. Discussion started: 10 November 2020

Atmospheric Measurement Techniques
Discussions

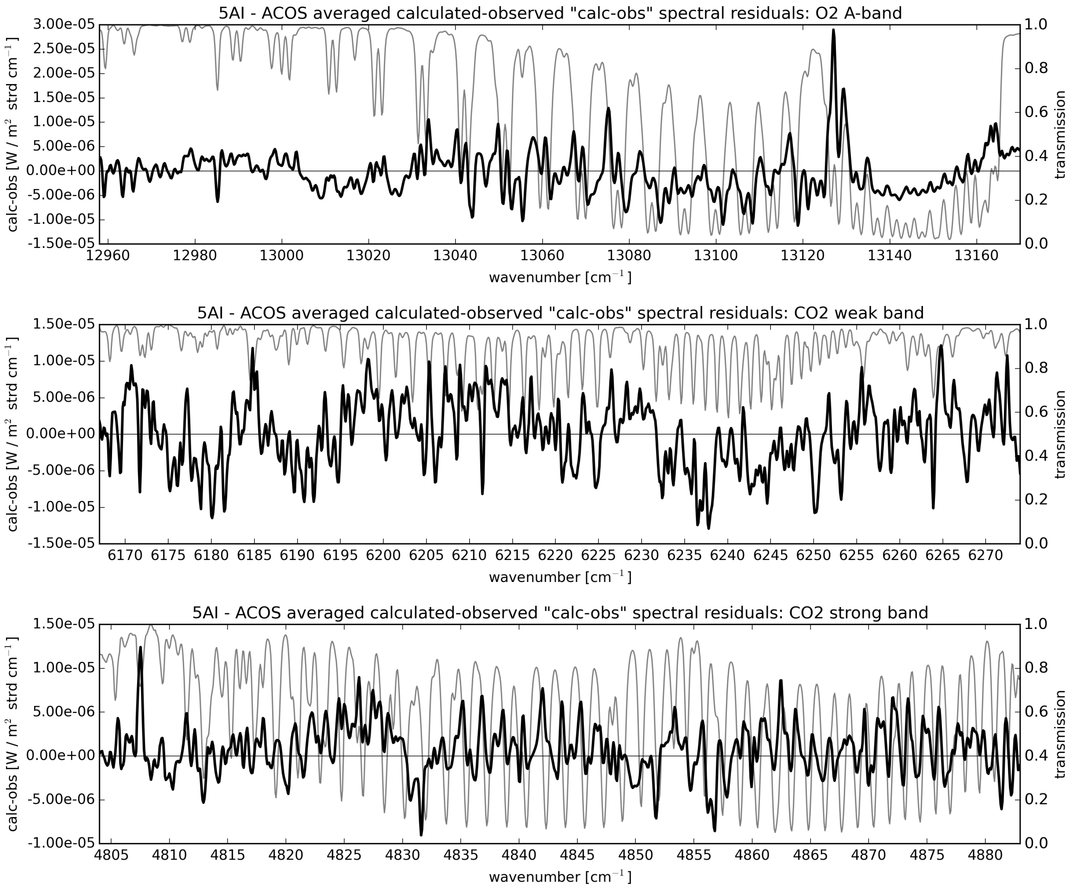

Figure 10. 5AI – ACOS average calculated – observed 'calc-obs' spectral residuals in the O_2 A-band (top panel), CO_2 weak band (middle panel) and CO_2 strong band (bottom panel) appear in thick black lines (left axis). Typical transmissions for the three bands are shown in thin grey lines (right axis).

In order to compare 5AI retrievals with ACOS products while attenuating the impact of the forward modelling differences, the obtained averaged calc – obs residual is added to every OCO-2 measurements within the complementary half of 2016 selected nadir soundings (6,799 in total) to compensate for the systematic radiative model differences between 4A/OP and ACOS. We then apply the 5AI inverse scheme on this new dataset. Figure 11 compares the distributions of 5AI – ACOS retrieval results obtained with and without the calc – obs adjustment. The systematic differences between 5AI and ACOS

https://doi.org/10.5194/amt-2020-403
Preprint. Discussion started: 10 November 2020

results for X_{H_2O}, X_{CO_2}, surface pressure and global temperature profile shift are fully removed when adding the spectral residual adjustment to OCO-2 measurements. This allows a first quantification of how spectroscopic and radiative transfer differences can impact X_{CO_2} retrievals. This calc – obs adjustment impacts the standard deviations of 5AI – ACOS differences. Indeed, several retrieval setup and forward modelling differences such as scattering particle parameters remain unaccounted for in this analysis. Their impact may be attenuated by the background difference correction, which, if disabled, leads to a similar standard deviation of 5AI – ACOS differences in both with and without calc – obs cases. However, without the background compensation, the average difference between 5AI – ACOS is only reduced to 1.9 ppm for X_{CO_2} (not shown). This exemplifies how highly challenging the sounding-to-sounding inter-comparison of retrieval results remains, and highlights how forward modelling and retrieval setup design impact X_{CO_2} retrieval results.

https://doi.org/10.5194/amt-2020-403
Preprint. Discussion started: 10 November 2020

Atmospheric Measurement Techniques
Discussions

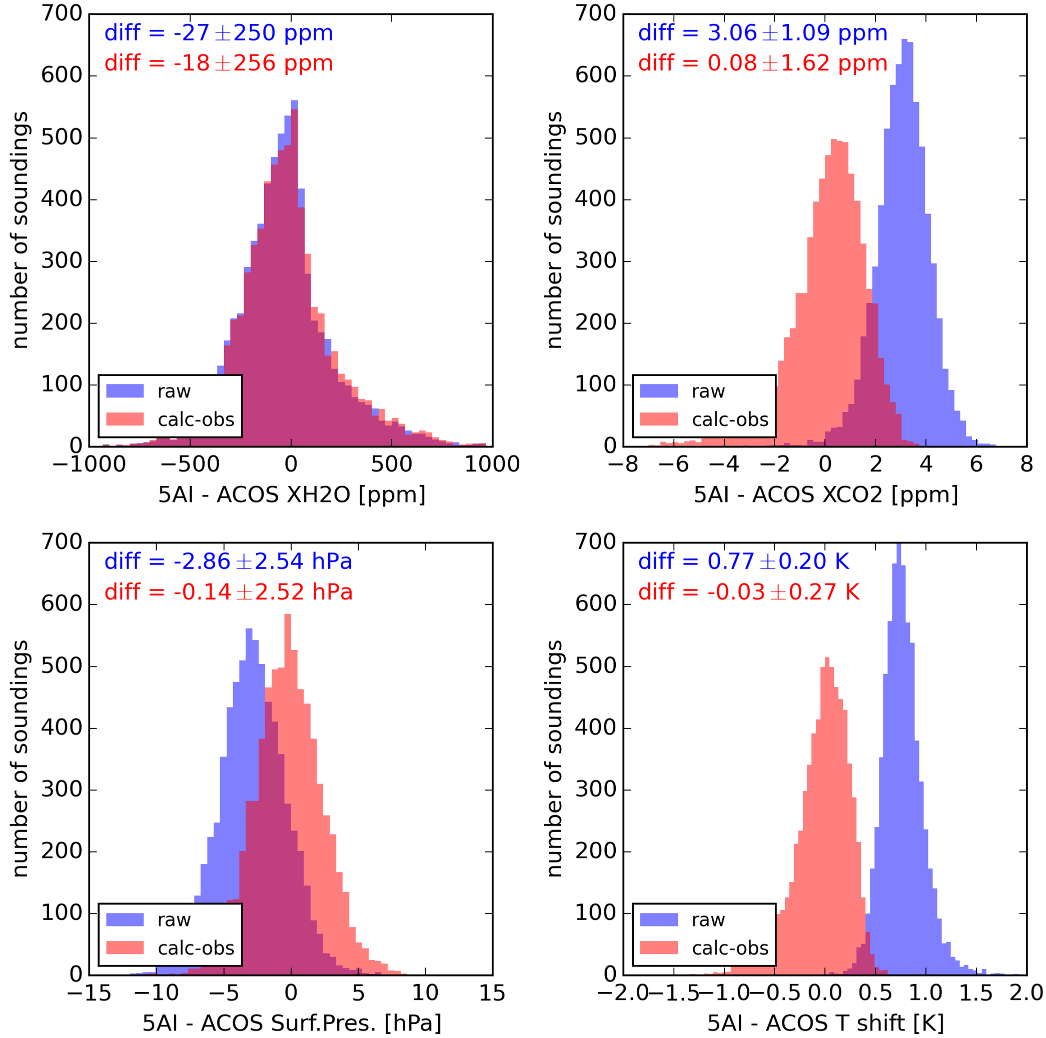

Figure 11. 5AI - raw ACOS B8r difference distributions for X_{H_2O} (top left), X_{CO_2} (top right), surface pressure (bottom left) and temperature profile global shift (bottom right) showed without applying the average calc-obs spectral residual correction (in blue) and with the correction (in red).

450

5. Conclusions

In this work, we have introduced the 5AI inverse scheme: it implements Bayesian optimal estimation and uses the 4A/OP radiative transfer model with the GEISA spectroscopic database and an empirically corrected absorption continuum in the O_2 A-band. We have applied the 5AI inverse scheme to retrieve X_{CO_2} from a sample of ~77k OCO-2 clear-sky soundings with low ACOS retrieved total AOD in target and nadir mode. Its global averaged uncorrected bias with regard to TCCON is 1.33 ppm with a standard deviation of 1.29 ppm for airmasses below 3.0. These results are comparable in standard deviation with those obtained by ACOS and FOCAL v08 for corresponding sets of OCO-2 soundings. Moreover, we showed that, similarly to ACOS, 5AI X_{CO_2} retrievals satisfactorily capture the global increasing trend of atmospheric CO_2, its seasonal cycle as well as its latitudinal variations, and that 5AI results are consistent between OCO-2 nadir and target modes. Although 5AI exhibits a difference of ~3 ppm with regard to ACOS, we showed that forward modelling differences between 5AI and ACOS can be removed with an average 'calculated – observed' spectral residual correction added to OCO-2 measurements, thus underlying the critical sensitivity of retrieval results to forward modelling.

For favourable conditions (clear sky, low ACOS total AOD), we showed that 5AI is a reliable implementation of the optimal estimation algorithm whose results can be compared to other available products. Efforts are underway in order to optimize and increase the speed of 4A/OP coupling with LIDORT and VLIDORT, and hence to process more soundings and account for cirrus clouds or aerosols in the retrievals. Additionally, 5AI retrieval setup will be refined to process soundings with airmasses larger than 3.0 in future works. Finally, the implementation of the 5AI retrieval scheme is intended to be compatible with 4A/OP structure, so that the code can be easily adapted to any current or future greenhouse gas monitoring instrument, from TCCON or EM27/SUN (e.g. Gisi et al., 2012; Hase et al., 2016) to OCO-2, MicroCarb (Pascal et al., 2017) or CO_2 Monitoring (Meijer and Team, 2019), and even applied to research concepts such as the one proposed in the European Commission H2020 SCARBO project (Brooker, 2018).

Data availability

For this work we use the B8r and B9r releases of OCO-2 data that were produced by the OCO-2 project at the Jet Propulsion Laboratory, California Institute of Technology, and obtained from the OCO-2 data archive maintained at the NASA Goddard Earth Science Data and Information Services Center (NASA GES-DISC). TCCON data are available on the TCCON Data Archive (https://tccondata.org/) and FOCAL v08 data can be downloaded on the FOCAL-OCO2 website hosted by the University of Bremen (http://www.iup.uni-bremen.de/~mreuter/focal.php). 5AI retrieval results presented in this work are available upon request from Matthieu Dogniaux by email (matthieu.dogniaux@lmd.ipsl.fr).

https://doi.org/10.5194/amt-2020-403
Preprint. Discussion started: 10 November 2020

Atmospheric Measurement Techniques
Discussions

Competing interests

The authors declare that they have no conflict of interest.

Acknowledgements

This work has received funding from CNES and CNRS. M. Dogniaux is funded by Airbus Defence and Space in the framework of a scientific collaboration with École polytechnique. The authors would like to thank the ACOS team and NASA for OCO-2 data availability as well as Maximilian Reuter and the University of Bremen for FOCAL v08 data availability.

The TCCON site at Réunion Island is operated by the Royal Belgian Institute for Space Aeronomy with financial support since 2014 by the EU project ICOS-Inwire and the ministerial decree for ICOS (FR/35/IC1 to FR/35/C5) and local activities supported by LACy/UMR8105 – Université de La Réunion. The TCCON stations at Tsukuba and Burgos are supported in part by the GOSAT series project. Local support for Burgos is provided by the Energy Development Corporation (EDC, Philippines). The Paris TCCON site has received funding from Sorbonne Université, the French research center CNRS, the French space agency CNES, and Région Île-de-France. The Ascension Island TCCON station has been supported by the European Space Agency (ESA) under grant 4000120088/17/I-EF and by the German Bundesministerium für Wirtschaft und Energie (BMWi) under grants 50EE1711C and 50EE1711E. We thank the ESA Ariane Tracking Station at North East Bay, Ascension Island, for hosting and local support. N. Deutscher is funded by ARC Future Fellowship FT180100327. Darwin and Wollongong TCCON stations are supported by ARC grants DP160100598, LE0668470, DP140101552, DP110103118 and DP0879468 and NASA grants NAG5-12247 and NNG05-GD07G.

References

Basu, S., Guerlet, S., Butz, A., Houweling, S., Hasekamp, O., Aben, I., Krummel, P., Steele, P., Langenfelds, R., Torn, M., Biraud, S., Stephens, B., Andrews, A. and Worthy, D.: Global CO2 fluxes estimated from GOSAT retrievals of total column CO2, Atmos. Chem. Phys., 13(17), 8695–8717, doi:10.5194/acp-13-8695-2013, 2013.

Basu, S., Baker, D. F., Chevallier, F., Patra, P. K., Liu, J. and Miller, J. B.: The impact of transport model differences on CO2 surface flux estimates from OCO-2 retrievals of column average CO2, Atmos. Chem. Phys., 18(10), 7189–7215, doi:10.5194/acp-18-7189-2018, 2018.

Blumenstock, T., Hase, F., Schneider, M., García, O. E. and Sepúlveda, E.: TCCON data from Izana (ES), Release GGG2014.R1, , doi:10.14291/TCCON.GGG2014.IZANA01.R1, 2017.

Bösch, H., Toon, G. C., Sen, B., Washenfelder, R. A., Wennberg, P. O., Buchwitz, M., de Beek, R., Burrows, J. P., Crisp, D., Christi, M., Connor, B. J., Natraj, V. and Yung, Y. L.: Space-based near-infrared CO2 measurements: Testing the

Orbiting Carbon Observatory retrieval algorithm and validation concept using SCIAMACHY observations over Park Falls, Wisconsin, J. Geophys. Res. Atmos., 111(D23), doi:10.1029/2006JD007080, 2006.

Bovensmann, H., Burrows, J. P., Buchwitz, M., Frerick, J., Noël, S., Rozanov, V. V., Chance, K. V. and Goede, A. P. H.: SCIAMACHY: Mission objectives and measurement modes, J. Atmos. Sci., 56(2), 127–150, doi:10.1175/1520-0469(1999)056<0127:SMOAMM>2.0.CO;2, 1999.

Brooker, L.: CONSTELLATION OF SMALL SATELLITES FOR THE MONITORING OF GREENHOUSE GASES, in 69th International Astronautical Congress (IAC)., 2018.

Buchwitz, M., Rozanov, V. V and Burrows, J. P.: A correlated-k distribution scheme for overlapping gases suitable for retrieval of atmospheric constituents from moderate resolution radiance measurements in the visible/near-infrared spectral region, J. Geophys. Res. Atmos., 105(D12), 15247–15261, doi:10.1029/2000JD900171, 2000.

Buchwitz, M., de Beek, R., Burrows, J. P., Bovensmann, H., Warneke, T., Notholt, J., Meirink, J. F., Goede, A. P. H., Bergamaschi, P., Körner, S., Heimann, M. and Schulz, A.: Atmospheric methane and carbon dioxide from SCIAMACHY satellite data: initial comparison with chemistry and transport models, Atmos. Chem. Phys., 5(4), 941–962, doi:10.5194/acp-5-941-2005, 2005.

Butz, A., Guerlet, S., Hasekamp, O., Schepers, D., Galli, A., Aben, I., Frankenberg, C., Hartmann, J.-M., Tran, H., Kuze, A., Keppel-Aleks, G., Toon, G., Wunch, D., Wennberg, P., Deutscher, N., Griffith, D., Macatangay, R., Messerschmidt, J., Notholt, J. and Warneke, T.: Toward accurate CO2 and CH4 observations from GOSAT, Geophys. Res. Lett., 38(14), doi:10.1029/2011GL047888, 2011.

Chédin, A., Serrar, S., Scott, N. A., Crevoisier, C. and Armante, R.: First global measurement of midtropospheric CO2 from NOAA polar satellites: Tropical zone, J. Geophys. Res. Atmos., 108(D18), doi:10.1029/2003JD003439, 2003.

Cheruy, F., Scott, N. A., Armante, R., Tournier, B. and Chedin, A.: Contribution to the development of radiative transfer models for high spectral resolution observations in the infrared, J. Quant. Spectrosc. Radiat. Transf., 53(6), 597–611, doi:https://doi.org/10.1016/0022-4073(95)00026-H, 1995.

Chevallier, F., Bréon, F.-M. and Rayner, P. J.: Contribution of the Orbiting Carbon Observatory to the estimation of CO2 sources and sinks: Theoretical study in a variational data assimilation framework, J. Geophys. Res. Atmos., 112(D9), doi:10.1029/2006JD007375, 2007.

Connor, B. J., Boesch, H., Toon, G., Sen, B., Miller, C. and Crisp, D.: Orbiting Carbon Observatory: Inverse method and prospective error analysis, J. Geophys. Res. Atmos., 113(D5), doi:10.1029/2006JD008336, 2008.

Crevoisier, C., Heilliette, S., Chédin, A., Serrar, S., Armante, R. and Scott, N. A.: Midtropospheric CO2 concentration retrieval from AIRS observations in the tropics, Geophys. Res. Lett., 31(17), doi:10.1029/2004GL020141, 2004.

Crevoisier, C., Chédin, A., Matsueda, H., Machida, T., Armante, R. and Scott, N. A.: First year of upper tropospheric integrated content of CO2 from IASI hyperspectral infrared observations, Atmos. Chem. Phys., 9(14), 4797–4810, doi:10.5194/acp-9-4797-2009, 2009a.

Crevoisier, C., Nobileau, D., Fiore, A. M., Armante, R., Chédin, A. and Scott, N. A.: Tropospheric methane in the tropics –

https://doi.org/10.5194/amt-2020-403
Preprint. Discussion started: 10 November 2020

first year from IASI hyperspectral infrared observations, Atmos. Chem. Phys., 9(17), 6337–6350, doi:10.5194/acp-9-6337-2009, 2009b.

Crevoisier, C., Clerbaux, C., Guidard, V., Phulpin, T., Armante, R., Barret, B., Camy-Peyret, C., Chaboureau, J.-P., Coheur, P.-F., Crépeau, L., Dufour, G., Labonnote, L., Lavanant, L., Hadji-Lazaro, J., Herbin, H., Jacquinet-Husson, N., Payan, S., Péquignot, E., Pierangelo, C., Sellitto, P. and Stubenrauch, C.: Towards IASI-New Generation (IASI-NG): impact of improved spectral resolution and radiometric noise on the retrieval of thermodynamic, chemistry and climate variables, Atmos. Meas. Tech., 7(12), 4367–4385, doi:10.5194/amt-7-4367-2014, 2014.

Crisp, D., Pollock, H. R., Rosenberg, R., Chapsky, L., Lee, R. A. M., Oyafuso, F. A., Frankenberg, C., O'Dell, C. W., Bruegge, C. J., Doran, G. B., Eldering, A., Fisher, B. M., Fu, D., Gunson, M. R., Mandrake, L., Osterman, G. B., Schwandner, F. M., Sun, K., Taylor, T. E., Wennberg, P. O. and Wunch, D.: The on-orbit performance of the Orbiting Carbon Observatory-2 (OCO-2) instrument and its radiometrically calibrated products, Atmos. Meas. Tech., 10(1), 59–81, doi:10.5194/amt-10-59-2017, 2017.

Deutscher, N. M., Notholt, J., Messerschmidt, J., Weinzierl, C., Warneke, T., Petri, C. and Grupe, P.: TCCON data from Bialystok (PL), Release GGG2014.R2, , doi:10.14291/TCCON.GGG2014.BIALYSTOK01.R2, 2019.

Drouin, B. J., Benner, D. C., Brown, L. R., Cich, M. J., Crawford, T. J., Devi, V. M., Guillaume, A., Hodges, J. T., Mlawer, E. J., Robichaud, D. J., Oyafuso, F., Payne, V. H., Sung, K., Wishnow, E. H. and Yu, S.: Multispectrum analysis of the oxygen A-band, J. Quant. Spectrosc. Radiat. Transf., 186, 118–138, doi:https://doi.org/10.1016/j.jqsrt.2016.03.037, 2017.

Duan, M., Min, Q. and Li, J.: A fast radiative transfer model for simulating high-resolution absorption bands, J. Geophys. Res. Atmos., 110(D15), doi:10.1029/2004JD005590, 2005.

Ehret, G., Bousquet, P., Pierangelo, C., Alpers, M., Millet, B., Abshire, J., Bovensmann, H., Burrows, J., Chevallier, F., Ciais, P. and et al.: MERLIN: A French-German Space Lidar Mission Dedicated to Atmospheric Methane, Remote Sens., 9(10), 1052, doi:10.3390/rs9101052, 2017.

Feist, D. G., Arnold, S. G., John, N. and Geibel, M. C.: TCCON data from Ascension Island (SH), Release GGG2014.R0, , doi:10.14291/TCCON.GGG2014.ASCENSION01.R0/1149285, 2014.

Gisi, M., Hase, F., Dohe, S., Blumenstock, T., Simon, A. and Keens, A.: XCO2 measurements with a tabletop FTS using solar absorption spectroscopy, Atmos. Meas. Tech., 5(11), 2969–2980, doi:10.5194/amt-5-2969-2012, 2012.

Griffith, D. W. T., Deutscher, N. M., Velazco, V. A., Wennberg, P. O., Yavin, Y., Keppel-Aleks, G., Washenfelder, R. A., Toon, G. C., Blavier, J.-F., Paton-Walsh, C., Jones, N. B., Kettlewell, G. C., Connor, B. J., Macatangay, R. C., Roehl, C., Ryczek, M., Glowacki, J., Culgan, T. and Bryant, G. W.: TCCON data from Darwin (AU), Release GGG2014.R0, , doi:10.14291/TCCON.GGG2014.DARWIN01.R0/1149290, 2014a.

Griffith, D. W. T., Velazco, V. A., Deutscher, N. M., Paton-Walsh, C., Jones, N. B., Wilson, S. R., Macatangay, R. C., Kettlewell, G. C., Buchholz, R. R. and Riggenbach, M. O.: TCCON data from Wollongong (AU), Release GGG2014.R0, , doi:10.14291/TCCON.GGG2014.WOLLONGONG01.R0/1149291, 2014b.

Hase, F., Blumenstock, T., Dohe, S., Groß, J. and Kiel, M. ä.: TCCON data from Karlsruhe (DE), Release GGG2014.R1, , doi:10.14291/TCCON.GGG2014.KARLSRUHE01.R1/1182416, 2015.

Hase, F., Frey, M., Kiel, M., Blumenstock, T., Harig, R., Keens, A. and Orphal, J.: Addition of a channel for XCO observations to a portable FTIR spectrometer for greenhouse gas measurements, Atmos. Meas. Tech., 9(5), 2303–2313, doi:10.5194/amt-9-2303-2016, 2016.

Hasekamp, O. P. and Landgraf, J.: A linearized vector radiative transfer model for atmospheric trace gas retrieval, J. Quant. Spectrosc. Radiat. Transf., 75(2), 221–238, doi:https://doi.org/10.1016/S0022-4073(01)00247-3, 2002.

Inoue, M., Morino, I., Uchino, O., Nakatsuru, T., Yoshida, Y., Yokota, T., Wunch, D., Wennberg, P. O., Roehl, C. M., Griffith, D. W. T., Velazco, V. A., Deutscher, N. M., Warneke, T., Notholt, J., Robinson, J., Sherlock, V., Hase, F., Blumenstock, T., Rettinger, M., Sussmann, R., Kyrö, E., Kivi, R., Shiomi, K., Kawakami, S., De Mazière, M., Arnold, S. G., Feist, D. G., Barrow, E. A., Barney, J., Dubey, M., Schneider, M., Iraci, L. T., Podolske, J. R., Hillyard, P. W., Machida, T., Sawa, Y., Tsuboi, K., Matsueda, H., Sweeney, C., Tans, P. P., Andrews, A. E., Biraud, S. C., Fukuyama, Y., Pittman, J. V, Kort, E. A. and Tanaka, T.: Bias corrections of GOSAT SWIR XCO2 and XCH4 with TCCON data and their evaluation using aircraft measurement data, Atmos. Meas. Tech., 9(8), 3491–3512, doi:10.5194/amt-9-3491-2016, 2016.

Iraci, L. T., Podolske, J. R., Hillyard, P. W., Roehl, C., Wennberg, P. O., Blavier, J.-F., Landeros, J., Allen, N., Wunch, D., Zavaleta, J., Quigley, E., Osterman, G. B., Albertson, R., Dunwoody, K. and Boyden, H.: TCCON data from Edwards (US), Release GGG2014.R1, , doi:10.14291/TCCON.GGG2014.EDWARDS01.R1/1255068, 2016.

Jacquinet-Husson, N., Armante, R., Scott, N. A., Chédin, A., Crépeau, L., Boutammine, C., Bouhdaoui, A., Crevoisier, C., Capelle, V., Boonne, C., Poulet-Crovisier, N., Barbe, A., Benner], D. [Chris, Boudon, V., Brown, L. R., Buldyreva, J., Campargue, A., Coudert, L. H., Devi, V. M., Down, M. J., Drouin, B. J., Fayt, A., Fittschen, C., Flaud, J.-M., Gamache, R. R., Harrison, J. J., Hill, C., Hodnebrog, Ø., Hu, S.-M., Jacquemart, D., Jolly, A., Jiménez, E., Lavrentieva, N. N., Liu, A.-W., Lodi, L., Lyulin, O. M., Massie, S. T., Mikhailenko, S., Müller, H. S. P., Naumenko, O. V, Nikitin, A., Nielsen, C. J., Orphal, J., Perevalov, V. I., Perrin, A., Polovtseva, E., Predoi-Cross, A., Rotger, M., Ruth, A. A., Yu, S. S., Sung, K., Tashkun, S. A., Tennyson, J., Tyuterev, V. G., Auwera], J. [Vander, Voronin, B. A. and Makie, A.: The 2015 edition of the GEISA spectroscopic database, J. Mol. Spectrosc., 327, 31–72, doi:https://doi.org/10.1016/j.jms.2016.06.007, 2016.

Kawakami, S., Ohyama, H., Arai, K., Okumura, H., Taura, C., Fukamachi, T. and Sakashita, M.: TCCON data from Saga (JP), Release GGG2014.R0, , doi:10.14291/TCCON.GGG2014.SAGA01.R0/1149283, 2014.

Kiel, M., O'Dell, C. W., Fisher, B., Eldering, A., Nassar, R., MacDonald, C. G. and Wennberg, P. O.: How bias correction goes wrong: measurement of XCO2 affected by erroneous surface pressure estimates, Atmos. Meas. Tech., 12(4), 2241–2259, doi:10.5194/amt-12-2241-2019, 2019.

Kivi, R. and Heikkinen, P.: Fourier transform spectrometer measurements of column CO2 at Sodankylä, Finland, Geosci. Instrumentation, Methods Data Syst., 5(2), 271–279, doi:10.5194/gi-5-271-2016, 2016.

Kivi, R., Heikkinen, P. and Kyrö, E.: TCCON data from Sodankylä (FI), Release GGG2014.R0, , doi:10.14291/TCCON.GGG2014.SODANKYLA01.R0/1149280, 2014.

Lamouroux, J., Tran, H., Laraia, A. L., Gamache, R. R., Rothman, L. S., Gordon, I. E. and Hartmann, J.-M.: Updated database plus software for line-mixing in CO2 infrared spectra and their test using laboratory spectra in the 1.5–2.3µm region, J. Quant. Spectrosc. Radiat. Transf., 111(15), 2321–2331, doi:https://doi.org/10.1016/j.jqsrt.2010.03.006, 2010.

De Mazière, M., Sha, M. K., Desmet, F., Hermans, C., Scolas, F., Kumps, N., Metzger, J.-M., Duflot, V. and Cammas, J.-P.: TCCON data from Réunion Island (RE), Release GGG2014.R1, , doi:10.14291/TCCON.GGG2014.REUNION01.R1, 2017.

Meijer, Y. and Team, C.: Copernicus CO2 Monitoring Mission Requirements Document. [online] Available from: https://esamultimedia.esa.int/docs/EarthObservation/CO2M_MRD_v2.0_Issued20190927.pdf, 2019.

Morino, I., Velazco, V. A., Hori, A., Uchino, O. and Griffith, D. W. T.: TCCON data from Burgos, Ilocos Norte (PH), Release GGG2014.R0, , doi:10.14291/TCCON.GGG2014.BURGOS01.R0, 2018a.

Morino, I., Matsuzaki, T. and Horikawa, M.: TCCON data from Tsukuba (JP), 125HR, Release GGG2014.R2, , doi:10.14291/TCCON.GGG2014.TSUKUBA02.R2, 2018b.

Natraj, V., Boesch, H., Spurr, R. J. D. and Yung, Y. L.: Retrieval of from simulated Orbiting Carbon Observatory measurements using the fast linearized R-2OS radiative transfer model, J. Geophys. Res. Atmos., 113(D11), doi:10.1029/2007JD009017, 2008.

Nguyen, H., Osterman, G., Wunch, D., O'Dell, C., Mandrake, L., Wennberg, P., Fisher, B. and Castano, R.: A method for colocating satellite XCO2 data to ground-based data and its application to ACOS-GOSAT and TCCON, Atmos. Meas. Tech., 7(8), 2631–2644, doi:10.5194/amt-7-2631-2014, 2014.

Notholt, J., Petri, C., Warneke, T., Deutscher, N. M., Palm, M., Buschmann, M., Weinzierl, C., Macatangay, R. C. and Grupe, P.: TCCON data from Bremen (DE), Release GGG2014.R0, , doi:10.14291/TCCON.GGG2014.BREMEN01.R0/1149275, 2014.

O'Dell, C. W., Connor, B., Bösch, H., O'Brien, D., Frankenberg, C., Castano, R., Christi, M., Eldering, D., Fisher, B., Gunson, M., McDuffie, J., Miller, C. E., Natraj, V., Oyafuso, F., Polonsky, I., Smyth, M., Taylor, T., Toon, G. C., Wennberg, P. O. and Wunch, D.: The ACOS CO2 retrieval algorithm – Part 1: Description and validation against synthetic observations, Atmos. Meas. Tech., 5(1), 99–121, doi:10.5194/amt-5-99-2012, 2012.

O'Dell, C. W., Eldering, A., Wennberg, P. O., Crisp, D., Gunson, M. R., Fisher, B., Frankenberg, C., Kiel, M., Lindqvist, H., Mandrake, L., Merrelli, A., Natraj, V., Nelson, R. R., Osterman, G. B., Payne, V. H., Taylor, T. E., Wunch, D., Drouin, B. J., Oyafuso, F., Chang, A., McDuffie, J., Smyth, M., Baker, D. F., Basu, S., Chevallier, F., Crowell, S. M. R., Feng, L., Palmer, P. I., Dubey, M., Garc\'\ia, O. E., Griffith, D. W. T., Hase, F., Iraci, L. T., Kivi, R., Morino, I., Notholt, J., Ohyama, H., Petri, C., Roehl, C. M., Sha, M. K., Strong, K., Sussmann, R., Te, Y., Uchino, O. and Velazco, V. A.: Improved retrievals of carbon dioxide from Orbiting Carbon Observatory-2 with the version 8 ACOS algorithm, Atmos. Meas. Tech., 11(12), 6539–6576, doi:10.5194/amt-11-6539-2018, 2018.

Oyafuso, F., Payne, V. H., Drouin, B. J., Devi, V. M., Benner, D. C., Sung, K., Yu, S., Gordon, I. E., Kochanov, R., Tan, Y., Crisp, D., Mlawer, E. J. and Guillaume, A.: High accuracy absorption coefficients for the Orbiting Carbon Observatory-2 (OCO-2) mission: Validation of updated carbon dioxide cross-sections using atmospheric spectra, J. Quant. Spectrosc. Radiat. Transf., 203, 213–223, doi:https://doi.org/10.1016/j.jqsrt.2017.06.012, 2017.

https://doi.org/10.5194/amt-2020-403
Preprint. Discussion started: 10 November 2020

Parker, R., Boesch, H., Cogan, A., Fraser, A., Feng, L., Palmer, P. I., Messerschmidt, J., Deutscher, N., Griffith, D. W. T., Notholt, J., Wennberg, P. O. and Wunch, D.: Methane observations from the Greenhouse Gases Observing SATellite: Comparison to ground-based TCCON data and model calculations, Geophys. Res. Lett., 38(15), doi:10.1029/2011GL047871, 2011.

Pascal, V., Buil, C., Loesel, J., Tauziede, L., Jouglet, D. and Buisson, F.: An improved microcarb dispersive instrumental concept for the measurement of greenhouse gases concentration in the atmosphere, in International Conference on Space Optics — ICSO 2014, vol. 10563, edited by Z. Sodnik, B. Cugny, and N. Karafolas, pp. 1028–1036, SPIE., 2017.

Le Quéré, C., Raupach, M., Canadell, J., Marland, G., Bopp, L., Ciais, P., Conway, T., Doney, S., Feely, R., Foster, P., Friedlingstein, P., Gurney, K., Houghton, R., House, J., Huntingford, C., Levy, P., Lomas, M., Majkut, J., Metzl, N. and Woodward, I.: Trends in the sources and sinks of carbon dioxide, Nat. Geosci., 2, 831–836, doi:10.1038/ngeo689, 2009.

Rayner, P. J. and O'Brien, D. M.: The utility of remotely sensed CO2 concentration data in surface source inversions, Geophys. Res. Lett., 28(1), 175–178, doi:10.1029/2000GL011912, 2001.

Reuter, M., Buchwitz, M., Schneising, O., Heymann, J., Bovensmann, H. and Burrows, J. P.: A method for improved SCIAMACHY CO2 retrieval in the presence of optically thin clouds, Atmos. Meas. Tech., 3(1), 209–232, doi:10.5194/amt-3-209-2010, 2010.

Reuter, M., Bovensmann, H., Buchwitz, M., Burrows, J. P., Connor, B. J., Deutscher, N. M., Griffith, D. W. T., Heymann, J., Keppel-Aleks, G., Messerschmidt, J., Notholt, J., Petri, C., Robinson, J., Schneising, O., Sherlock, V., Velazco, V., Warneke, T., Wennberg, P. O. and Wunch, D.: Retrieval of atmospheric CO2 with enhanced accuracy and precision from SCIAMACHY: Validation with FTS measurements and comparison with model results, J. Geophys. Res. Atmos., 116(D4), doi:10.1029/2010JD015047, 2011.

Reuter, M., Buchwitz, M., Schneising, O., Noël, S., Rozanov, V., Bovensmann, H. and Burrows, J.: A Fast Atmospheric Trace Gas Retrieval for Hyperspectral Instruments Approximating Multiple Scattering—Part 1: Radiative Transfer and a Potential OCO-2 XCO2 Retrieval Setup, Remote Sens., 9(11), 1159, doi:10.3390/rs9111159, 2017a.

Reuter, M., Buchwitz, M., Schneising, O., Noël, S., Bovensmann, H. and Burrows, J.: A Fast Atmospheric Trace Gas Retrieval for Hyperspectral Instruments Approximating Multiple Scattering—Part 2: Application to XCO2 Retrievals from OCO-2, Remote Sens., 9(11), 1102, doi:10.3390/rs9111102, 2017b.

Rodgers, C. D.: Inverse Methods for Atmospheric Sounding, WORLD SCIENTIFIC., 2000.

Rothman, L. S., Gordon, I. E., Barbe, A., Benner, D. C., Bernath, P. F., Birk, M., Boudon, V., Brown, L. R., Campargue, A., Champion, J.-P., Chance, K., Coudert, L. H., Dana, V., Devi, V. M., Fally, S., Flaud, J.-M., Gamache, R. R., Goldman, A., Jacquemart, D., Kleiner, I., Lacome, N., Lafferty, W. J., Mandin, J.-Y., Massie, S. T., Mikhailenko, S. N., Miller, C. E., Moazzen-Ahmadi, N., Naumenko, O. V, Nikitin, A. V, Orphal, J., Perevalov, V. I., Perrin, A., Predoi-Cross, A., Rinsland, C. P., Rotger, M., Šimečková, M., Smith, M. A. H., Sung, K., Tashkun, S. A., Tennyson, J., Toth, R. A., Vandaele, A. C. and Auwera], J. [Vander: The HITRAN 2008 molecular spectroscopic database, J. Quant. Spectrosc. Radiat. Transf., 110(9), 533–572, doi:https://doi.org/10.1016/j.jqsrt.2009.02.013, 2009.

Rozanov, V. V, Buchwitz, M., Eichmann, K.-U., Beek], R. [de and Burrows, J. P.: Sciatran - a new radiative transfer model for geophysical applications in the 240–2400 NM spectral region: the pseudo-spherical version, Adv. Sp. Res., 29(11), 1831–1835, doi:https://doi.org/10.1016/S0273-1177(02)00095-9, 2002.

Rozanov, V. V, Rozanov, A. V, Kokhanovsky, A. A. and Burrows, J. P.: Radiative transfer through terrestrial atmosphere and ocean: Software package SCIATRAN, J. Quant. Spectrosc. Radiat. Transf., 133, 13–71, doi:https://doi.org/10.1016/j.jqsrt.2013.07.004, 2014.

Schepers, D., de Brugh], J. M. J. [aan, Hahne, P., Butz, A., Hasekamp, O. P. and Landgraf, J.: LINTRAN v2.0: A linearised vector radiative transfer model for efficient simulation of satellite-born nadir-viewing reflection measurements of cloudy atmospheres, J. Quant. Spectrosc. Radiat. Transf., 149, 347–359, doi:https://doi.org/10.1016/j.jqsrt.2014.08.019, 2014.

Scott, N. A. and Chédin, A.: A Fast Line-by-Line Method for Atmospheric Absorption Computations: The Automatized Atmospheric Absorption Atlas, J. Appl. Meteorol., 20(7), 802–812, 1981.

Sherlock, V., Connor, B., Robinson, J., Shiona, H., Smale, D. and Pollard, D. F.: TCCON data from Lauder (NZ), 125HR, Release GGG2014.R0, , doi:10.14291/TCCON.GGG2014.LAUDER02.R0/1149298, 2014.

Spurr, R. J. D.: Simultaneous derivation of intensities and weighting functions in a general pseudo-spherical discrete ordinate radiative transfer treatment, J. Quant. Spectrosc. Radiat. Transf., 75(2), 129–175, doi:https://doi.org/10.1016/S0022-4073(01)00245-X, 2002.

Spurr, R. J. D.: VLIDORT: A linearized pseudo-spherical vector discrete ordinate radiative transfer code for forward model and retrieval studies in multilayer multiple scattering media, J. Quant. Spectrosc. Radiat. Transf., 102(2), 316–342, doi:https://doi.org/10.1016/j.jqsrt.2006.05.005, 2006.

Strong, K., Roche, S., Franklin, J. E., Mendonca, J., Lutsch, E., Weaver, D., Fogal, P. F., Drummond, J. R., Batchelor, R. and Lindenmaier, R.: TCCON data from Eureka (CA), Release GGG2014.R3, , doi:10.14291/TCCON.GGG2014.EUREKA01.R3, 2019.

Té, Y., Jeseck, P. and Janssen, C.: TCCON data from Paris (FR), Release GGG2014.R0, , doi:10.14291/TCCON.GGG2014.PARIS01.R0/1149279, 2014.

Thompson, D. R., Benner], D. [Chris, Brown, L. R., Crisp, D., Devi], V. [Malathy, Jiang, Y., Natraj, V., Oyafuso, F., Sung, K., Wunch, D., Castaño, R. and Miller, C. E.: Atmospheric validation of high accuracy CO2 absorption coefficients for the OCO-2 mission, J. Quant. Spectrosc. Radiat. Transf., 113(17), 2265–2276, doi:https://doi.org/10.1016/j.jqsrt.2012.05.021, 2012.

Toon, G. C.: Solar Line List for the TCCON 2014 Data Release, , doi:10.14291/TCCON.GGG2014.SOLAR.R0/1221658, 2015.

Tournier: STRANSAC-93 et 4A-93: Développement et validation des nouvelles versions des codes de transfert radiatif pour application au projet IASI, PALAISEAU, France., 1995.

Tran, H. and Hartmann, J.-M.: An improved O2 A band absorption model and its consequences for retrievals of photon paths and surface pressures, J. Geophys. Res. Atmos., 113(D18), doi:10.1029/2008JD010011, 2008.

https://doi.org/10.5194/amt-2020-403
Preprint. Discussion started: 10 November 2020

Atmospheric Measurement Techniques Discussions

Warneke, T., Messerschmidt, J., Notholt, J., Weinzierl, C., Deutscher, N. M., Petri, C. and Grupe, P.: TCCON data from Orléans (FR), Release GGG2014.R1, , doi:10.14291/TCCON.GGG2014.ORLEANS01.R1, 2019.

Wennberg, P. O., Wunch, D., Roehl, C. M., Blavier, J.-F., Toon, G. C. and Allen, N. T.: TCCON data from Caltech (US), Release GGG2014.R1, , doi:10.14291/TCCON.GGG2014.PASADENA01.R1/1182415, 2015.

Wennberg, P. O., Wunch, D., Roehl, C. M., Blavier, J.-F., Toon, G. C. and Allen, N. T.: TCCON data from Lamont (US), Release GGG2014.R1, , doi:10.14291/TCCON.GGG2014.LAMONT01.R1/1255070, 2016.

Wennberg, P. O., Roehl, C. M., Wunch, D., Toon, G. C., Blavier, J.-F., Washenfelder, R., Keppel-Aleks, G., Allen, N. T. and Ayers, J.: TCCON data from Park Falls (US), Release GGG2014.R1, , doi:10.14291/TCCON.GGG2014.PARKFALLS01.R1, 2017.

Wu, L., Hasekamp, O., Hu, H., Landgraf, J., Butz, A., aan de Brugh, J., Aben, I., Pollard, D. F., Griffith, D. W. T., Feist, D. G., Koshelev, D., Hase, F., Toon, G. C., Ohyama, H., Morino, I., Notholt, J., Shiomi, K., Iraci, L., Schneider, M., de Mazière, M., Sussmann, R., Kivi, R., Warneke, T., Goo, T.-Y. and Té, Y.: Carbon dioxide retrieval from OCO-2 satellite observations using the RemoTeC algorithm and validation with TCCON measurements, Atmos. Meas. Tech., 11(5), 3111–3130, doi:10.5194/amt-11-3111-2018, 2018.

Wunch, D., Wennberg, P. O., Toon, G. C., Connor, B. J., Fisher, B., Osterman, G. B., Frankenberg, C., Mandrake, L., O'Dell, C., Ahonen, P., Biraud, S. C., Castano, R., Cressie, N., Crisp, D., Deutscher, N. M., Eldering, A., Fisher, M. L., Griffith, D. W. T., Gunson, M., Heikkinen, P., Keppel-Aleks, G., Kyrö, E., Lindenmaier, R., Macatangay, R., Mendonca, J., Messerschmidt, J., Miller, C. E., Morino, I., Notholt, J., Oyafuso, F. A., Rettinger, M., Robinson, J., Roehl, C. M., Salawitch, R. J., Sherlock, V., Strong, K., Sussmann, R., Tanaka, T., Thompson, D. R., Uchino, O., Warneke, T. and Wofsy, S. C.: A method for evaluating bias in global measurements of CO2 total columns from space, Atmos. Chem. Phys., 11(23), 12317–12337, doi:10.5194/acp-11-12317-2011, 2011a.

Wunch, D., Toon, G. C., Blavier, J.-F. L., Washenfelder, R. A., Notholt, J., Connor, B. J., Griffith, D. W. T., Sherlock, V. and Wennberg, P. O.: The Total Carbon Column Observing Network, Philos. Trans. R. Soc. A Math. Phys. Eng. Sci., 369(1943), 2087–2112, doi:10.1098/rsta.2010.0240, 2011b.

Wunch, D., Toon, G. C., Sherlock, V., Deutscher, N. M., Liu, C., Feist, D. G. and Wennberg, P. O.: The Total Carbon Column Observing Network's GGG2014 Data Version., 2015.

Wunch, D., Wennberg, P. O., Osterman, G., Fisher, B., Naylor, B., Roehl, C. M., O'Dell, C., Mandrake, L., Viatte, C., Kiel, M., Griffith, D. W. T., Deutscher, N. M., Velazco, V. A., Notholt, J., Warneke, T., Petri, C., De Maziere, M., Sha, M. K., Sussmann, R., Rettinger, M., Pollard, D., Robinson, J., Morino, I., Uchino, O., Hase, F., Blumenstock, T., Feist, D. G., Arnold, S. G., Strong, K., Mendonca, J., Kivi, R., Heikkinen, P., Iraci, L., Podolske, J., Hillyard, P. W., Kawakami, S., Dubey, M. K., Parker, H. A., Sepulveda, E., Garc\'\ia, O. E., Te, Y., Jeseck, P., Gunson, M. R., Crisp, D. and Eldering, A.: Comparisons of the Orbiting Carbon Observatory-2 (OCO-2) XCO2 measurements with TCCON, Atmos. Meas. Tech., 10(6), 2209–2238, doi:10.5194/amt-10-2209-2017, 2017.

Yokota, T., Yoshida, Y., Eguchi, N., Ota, Y., Tanaka, T., Watanabe, H. and Maksyutov, S.: Global Concentrations of CO2

https://doi.org/10.5194/amt-2020-403
Preprint. Discussion started: 10 November 2020

and CH_4 Retrieved from GOSAT: First Preliminary Results, SOLA, 5, 160–163, doi:10.2151/sola.2009-041, 2009.

Yoshida, Y., Ota, Y., Eguchi, N., Kikuchi, N., Nobuta, K., Tran, H., Morino, I. and Yokota, T.: Retrieval algorithm for CO_2 and CH_4 column abundances from short-wavelength infrared spectral observations by the Greenhouse gases observing satellite, Atmos. Meas. Tech., 4(4), 717–734, doi:10.5194/amt-4-717-2011, 2011.

Yoshida, Y., Kikuchi, N., Morino, I., Uchino, O., Oshchepkov, S., Bril, A., Saeki, T., Schutgens, N., Toon, G. C., Wunch, D., Roehl, C. M., Wennberg, P. O., Griffith, D. W. T., Deutscher, N. M., Warneke, T., Notholt, J., Robinson, J., Sherlock, V., Connor, B., Rettinger, M., Sussmann, R., Ahonen, P., Heikkinen, P., Kyrö, E., Mendonca, J., Strong, K., Hase, F., Dohe, S. and Yokota, T.: Improvement of the retrieval algorithm for GOSAT SWIR XCO_2 and XCH_4 and their validation using TCCON data, Atmos. Meas. Tech., 6(6), 1533–1547, doi:10.5194/amt-6-1533-2013, 2013.